Earth and Space Science

RESEARCH ARTICLE
10.1029/2024EA003844

Four Generations of ECMWF Reanalyses: An Overview of the Successes in Modeling Precipitation and Remaining Challenges for Freshwater Budget of Ocean Models

Raphael Dussin[1,2]

[1]National Oceanographic and Atmospheric Administration, Geophysical Fluid Dynamics Laboratory, Princeton, NJ, USA, [2]University Corporation for Atmospheric Research, Boulder, CO, USA

Key Points:

- The realism of precipitation has improved significantly in four generations of ECMWF reanalyses
- Regional metrics allow for a more comprehensive picture of the progress made in modeling precipitation
- ERA5 provides a better freshwater balance than ERA-Interim in a forced ocean general circulation model but challenges remain

Correspondence to:

R. Dussin,
raphael.dussin@noaa.gov

Citation:

Dussin, R. (2025). Four generations of ECMWF reanalyses: An overview of the successes in modeling precipitation and remaining challenges for freshwater budget of ocean models. *Earth and Space Science*, *12*, e2024EA003844. https://doi.org/10.1029/2024EA003844

Received 28 JUN 2024
Accepted 10 DEC 2024

Author Contribution:

Writing – original draft: Raphael Dussin
Writing – review & editing: Raphael Dussin

Abstract This study reviews the progress made in modeling precipitations in four generations of reanalyses from the European Center for Medium-Range Weather Forecasts, using traditional metrics and a new set of regional metrics. Regional metrics at oceanic basin scales and large land catchment areas over the continents allow for a more comprehensive analysis of the performance of the reanalyses. This leads to the conclusion that significant progress has been made in the past several decades in both the atmospheric model and the assimilation system at the ECMWF, leading to more realistic precipitation. The most recent ERA5 reanalysis outperforms ERA-Interim and its predecessors by all metrics considered. ERA5 is then used to force a modern ocean general circulation model, and the results show an improvement in terms of the freshwater budget, particularly after the year 2000. However, uncertainties remain about the magnitude and trends of the modeled evaporation.

1. Introduction

Modeling centers such as the European Center for Medium-Range Weather Forecasts (https://ecmwf.int), NOAA National Centers for Environmental Predictions (https://ncep.noaa.gov), NASA Global Modeling and Assimilation Office (https://gmao.gsfc.nasa.gov/) and Japan Meteorology Agency (http://jma.go.jp) are producing retrospective analyses of the atmosphere (hereafter reanalyses) using a fixed code base and assimilating quality controlled weather and satellite observational data streams in decades-long numerical integrations of their respective atmospheric models. These reanalyses provide very valuable atmospheric data sets and have become indispensable to atmospheric and climate science. They help to better understand trends and atmospheric variability on the interannual and decadal time scales and their impacts on the rest of the Earth system. The precipitation provided by atmospheric reanalyses is regularly scrutinized and compared with observations (e.g., Bukovsky & Karoly, 2007; Janowiak et al., 1998; Lee & Biasutti, 2014). Many studies focus on inter-comparing precipitation on land where observations are more readily available (e.g., Ghajarnia et al., 2022; Ning et al., 2016; Rivoire et al., 2021) to determine if these data sets are suitable to address specific scientific questions. Larger intercomparison projects (e.g., Hassler & Lauer, 2021; Sun et al., 2018; Tang et al., 2020) aim to quantify uncertainty at much larger spatial scales and identify the strengths and weaknesses of various reanalyses.

ECMWF is the only modeling center to publish four successive generations of atmospheric reanalyses, thus providing a unique opportunity to investigate the progress made by their Integrated Forecasting System (hereafter IFS) atmospheric model and data assimilation system in representing precipitation. The two other centers with two published reanalyses (JMA and NASA) have a shorter and more recent history, as they released their first generation, respectively, JRA-25 (Onogi et al., 2007) and MERRA (Rienecker et al., 2011), and their latest generation, JRA-55 (Kobayashi et al., 2015) and MERRA2 (Gelaro et al., 2017), within the same decade.

The first ECMWF reanalysis ERA15 was released at a time where global precipitation data sets were emerging, such as the first Global Precipitation Climatology Project (Arkin & Xie, 1994) and hence evaluation of its precipitation is limited. It was later replaced by ERA40, in which precipitation was analyzed and compared to observational estimates and highlighted the problem of excess rainfall in the tropics (Bosilovich et al., 2008). The subsequent ERA-Interim and ERA5 reanalyses were examined more thoroughly, and several studies show the overall good performance of ERA-Interim (e.g., Prakash et al., 2015; Sun et al., 2018) as well as improvements between ERA-Interim and ERA5 in the tropics (Li et al., 2021) and more broadly (Hassler & Lauer, 2021; Nogueira, 2020). Lavers et al. (2022) shows that ERA5 is skillful for climate monitoring in the extratropics, based

on an extensive comparison with land weather stations. Ocean precipitation data are sparse and ocean modelers often face the challenge of determining whether a precipitation data set is appropriate for their application.

The first objective of this article is to document the progress made by ECMWF reanalyses in modeling and assimilating precipitations over a period of 25 years since the release of ERA15 and up to the most recent ERA5. The metrics used to assess the quality of the modeled precipitation are separated into two categories: global and regional. Global metrics are commonly used in the climate modeling community and provide a first assessment of the strengths and weaknesses of various data sets. However, because precipitation has complex spatiotemporal characteristics, global metrics may not capture important features. Additional regional metrics allow for a more in-depth description of the progress made in representing precipitation and supplement global metrics. The second objective is to test whether the ERA5 precipitation is suitable to be used for the freshwater forcing of a modern ocean circulation model. Precipitation from previous generation of ECMWF reanalyses proved difficult to use without correction due to discrepancies in the spatial patterns and intensity. In ocean modeling applications, precipitation from reanalyses is often corrected using satellite-based observational estimates to address the most obvious spatial biases and create forcing data sets, such as CORE (Large & Yeager, 2004), JRA55do (Tsujino et al., 2018), Drakkar Forcing Sets (Brodeau et al., 2010; Dussin & Barnier, 2013). Various methods to correct precipitation to observational estimates have been proposed and are summarized in Dussin (2022). After correction, it is common to further adjust the total precipitation in order to close the freshwater budget of ocean models.

2. Characteristics of the Data Sets Used

2.1. Global Precipitation Climatology Project

This study uses Global Precipitation Climatology Project (hereafter GPCP) v2.3, described in Adler et al. (2018), as the ground truth: precipitation estimates are provided at a monthly frequency and 2.5° spatial resolution. GPCP uses a combination of satellite data and rain gauges to produce a monthly global data set. The choice of this product is motivated by the long time period available (1979–2020) and the global coverage. Other observation-based data sets, such as the Tropical Rainfall Measuring Mission (TRMM) (Huffman et al., 2007), have a finer temporal and spatial resolution, but a shorter time period and a limited geographical area. TRMM estimates a stronger precipitation than GPCP v2.3 in the Inter-Tropical Convergence Zone (ITCZ) by not more than 8% (see Figure 3 of Dussin (2022)). Version 3.2 of GPCP (Huffman et al., 2023) was discarded due to artifacts in the combined satellite-gauge precipitation field, particularly noticeable early in the timeseries. Another option is the CPC Merged Analysis of Precipitation (CMAP) precipitation data set, but it was not used here because the reference publication (Xie & Arkin, 1997) predates GPCP v2.3 by a decade and missing satellite values are filled using the NCEP1 reanalysis from Kalnay et al. (1996).

ECMWF has released over the years four generations of atmospheric reanalyses named ERA (for ECMWF REanalysis), starting from ERA15 in 1993 to the most recent ERA5, with ERA40 and ERA-Interim in between. The relevant characteristics of the atmosphere model and the data assimilation system are summarized in Table 1.

2.2. ERA15

ERA15 is the first interannual reanalysis produced by ECMWF after the "First GARP Global Experiment" (FGGE) proof of concept (Bengtsson & Kållberg, 1981). It was released in 1995 and covers the 1979–1993 period. The atmospheric model used is IFS version 13r4 with a T106L31 grid (125 km horizontal resolution, 31 vertical levels resolving up to 10 hPa/32 km). The data assimilation system is an Optimal Interpolation (hereafter OI) with no First Guess at Appropriate Time (hereafter FGAT) with a 6-hr window. Although the variational approach and FGAT schemes were already being used operationally in the mid-1990s, the computational cost was determined to be too expensive. Many details on the final configuration of ERA15 and the decisions that led to it can be found in the project report of Gibson et al. (1997).

2.3. ERA40

ERA40 is the successor to ERA15 released in 2002 and now covers the extended period of 1958–2002. The IFS version is 23r4 with a T159L60 grid (125 km horizontal resolution, 60 vertical levels resolving up to 0.1 hPa/65 km). It now uses the so-called "linear grid" with a semi-Lagrangian advection scheme, which strongly reduces

Table 1
Technical Characteristics of Atmospheric Model, Data Assimilation System and Grid Used for Each ERA Reanalysis

	ERA15	ERA40	ERAinterim	ERA5
Period	1979–1993	1958–2002	1979–2019	1940–2023
IFS version	13r4	23r4	31r2	41r2
DA type	OI-noFGAT	3d-var/FGAT	4d-var	4d-var
Horizontal resolution	125 km	125 km	80 km	31 km
Vertical resolution	31 levels	60 levels	60 levels	137 levels
Top height	32 km	65 km	65 km	80 km

the spectral ripples from the orography as shown in Figure 3 of Uppala et al. (2005). The data assimilation system has been changed to a 3d-var with FGAT with a 6-hr window, instead of the more expensive 4d-var used operationally. Uppala et al. (2005) report that better techniques in input data pre-processing and physical parameterizations are responsible for improvements over ERA15. However, it acknowledges issues with the humidity analysis spreading increments horizontally hence leading to excessive precipitations in the tropical oceans. Moreover, the satellite radiances were misinterpreted after the eruption of Mount Pinatubo, resulting in exaggerated rainfall rates in the 1990s.

2.4. ERA-Interim

ERA-Interim (abbreviated ERAi in the figures), as the name suggests, was intended to be a provisional product until the newest ECMWF reanalysis was produced. It originally covered the 1989–2004 period but was later extended backward and forward to 1979–2019. The IFS version is 31r2 with a T255L60 grid (80 km horizontal resolution, 60 vertical levels resolving up to 0.1 hPa/65 km). The assimilation system is upgraded to a 4d-var with a 12-hr window, like the one used operationally. In addition to an increase in horizontal resolution and changes in the model's physics, the major upgrade of ERA-Interim is the addition of the fully automated adaptative bias correction for satellite radiances from Dee (2004) and a new humidity analysis. However, the global mean precipitation shows several jumps that Dee et al. (2011) attribute to problems with the 1D+4D variational rain assimilation system.

2.5. ERA5

ERA5 is the fourth generation of ECMWF reanalyses and the latest to date, covers the 1979 to present (2023) period and is extended back to 1940 (not used here). The IFS model is 41r2 with a T639L137 grid (31km horizontal resolution, 137 vertical levels to 0.01 hPa/80 km). The assimilation system is again the 4d-var ensemble with a 12-hr window. The many improvements to the model's physics and data assimilation are described in Hersbach et al. (2020). Their comparison with the TRMM data set (Huffman et al., 2007) shows an improvement in precipitation between ERA-Interim and ERA5, with an overall correlation increasing from 63% in ERA-Interim to 70% in ERA5. They acknowledge occurrences of “rain bombs” happening in very specific conditions over orographic areas (around 10 times/year, mostly over Africa) and that the problem was later solved in the operational system using an octahedral reduced Gaussian grid.

3. Results

This section is divided into three parts: The first part focuses on global metrics commonly used in the ocean and climate modeling community and used to describe the large-scale properties of the different data sets, including biases and trends. To investigate in more depth, the second part is a regional analysis that focuses on the representation of the seasonal cycle, interannual variability, and trends for each of the Sixth Assessment Report (AR6) regions defined by Iturbide et al. (2020). Finally, the third part explores the use of ERA5 to force a modern ocean general circulation model and the resulting freshwater balance. Some data sets include partial years; they are omitted for all metrics.

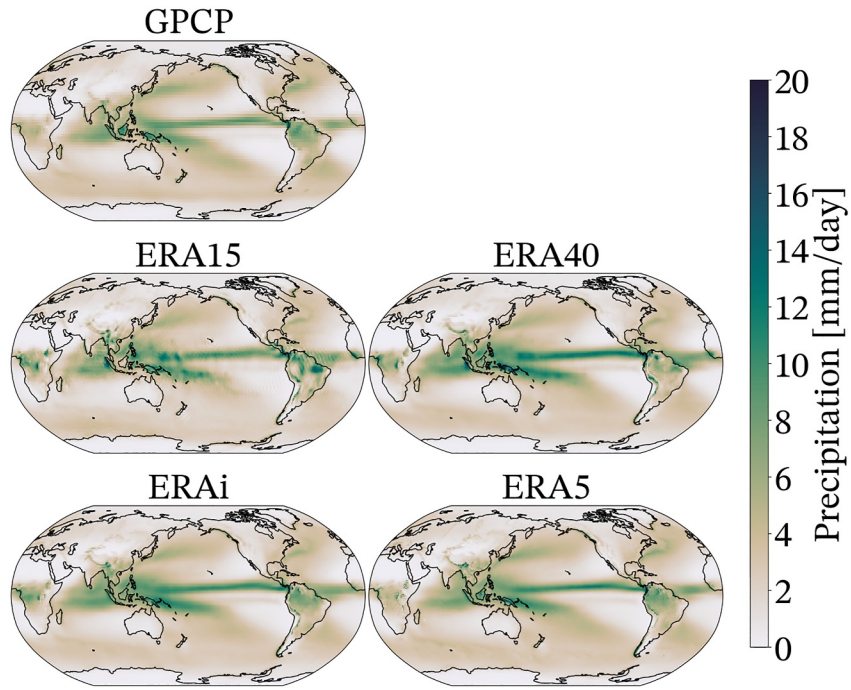

Figure 1. Climatological annual mean precipitation for observation-based estimates GPCP v2.3 (1979–2020), and modeled in the ECMWF reanalyses: ERA15 (1979–1993), ERA40 (1958–2001), ERA-Interim (1979–2018) and ERA5 (1979–2022). All data sets are presented at their native resolutions.

3.1. Global Analysis

The annual average is characterized by the ITCZ, a band of intense precipitation located just north of the equator and extending over the three tropical oceans (Pacific, Atlantic, and Indian). The year-round maximum insolation over the tropical oceans and rainforests leads to strong evaporation, deep convection, and therefore intense precipitation, in excess of 8 mm/day on annual average. In the southern hemisphere, two regions present precipitation exceeding 5 mm/day: the first is located in the western Pacific off the maritime continent and is named the South Pacific Convergence Zone (SPCZ). The second is located off the coast of Brazil and Argentina and is known as the South Atlantic Convergence Zone. In the northern hemisphere, the highest rainfall is found over western boundary currents (Gulf Stream and Kuroshio), where warm oceanic waters release some of the highest amount of latent heat to the atmosphere (order of magnitude of 200 W/m^2 annually), leading to precipitation bands following the path of the currents. The lowest precipitation can be found in the subtropics in the subsidence zones, located in the eastern part of the ocean basins. Figure 1 shows the climatological average (over all available years) of total precipitations in the GPCP observation-based data set and the ECMWF reanalyses. All of the latter successfully reproduce the main precipitation patterns and do not suffer from the double-ITCZ problem that plagues a number of climate models (Tian & Dong, 2020). However, it is apparent that the amplitudes are not always well captured and are particularly overestimated in the ITCZ and SPCZ. On land, the Amazon basin and Central Africa (CAF) are too wet, while Borneo and the northern Andes are too dry, particularly in ERA15 and ERA40.

To further compare between ERA and GPCP, precipitation data sets are remapped using the ESMF library (Hill et al., 2004). Figure 2 shows the mean biases between the reanalyses and GPCP. In this figure, the GPCP data set is remapped using a bilinear scheme from its coarse 2.5° resolution to the higher resolution of the IFS grids (1.125° for ERA15 and ERA40, 0.7° for ERA-Interim and 0.25° for ERA5). This allows showing small-scale details that would otherwise be smoothed out, such as spectral ripples in ERA15. However, since bilinear interpolation does not conserve spatial variance, the statistics are computed using ERA data sets coarsened onto the GPCP grid (not shown) with a conservative remapping scheme.

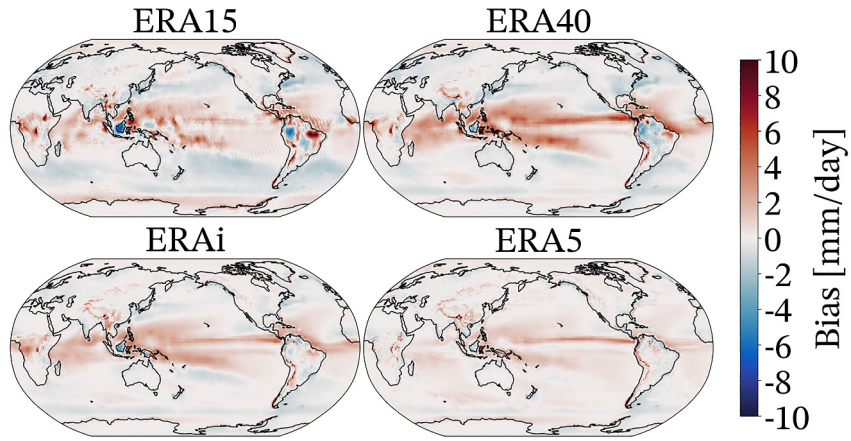

Figure 2. Climatological annual mean precipitation biases relative to GPCP in ERA15 (1979–1993), ERA40 (1979–2001), ERA-Interim (1979–2018) and ERA5 (1979–2020). Data from GPCP is remapped onto the various ERA native grids using bilinear interpolation. Difference is computed over the common period between the reanalysis and GPCP.

The successive generations of reanalyses show remarkable consistency in the spatial pattern of mean bias: precipitation in the ITCZ is overestimated in all cases, the SPCZ is too zonal (resulting in a dipole pattern in bias maps), and too much rain is produced north of the equator in the western Pacific and Atlantic oceans. On the contrary, precipitation is biased low at mid-latitudes and in the main western boundary currents of the northern hemisphere, except for ERA5. Although the bias pattern remains similar between all reanalyses, the amplitude differs between each successive generation. The mean bias increases from 0.13 mm/day (approximately 5% of the global average) in ERA15 to 0.32 mm/day (approximately 12%) in ERA40 due to a large increase in tropical precipitation. Because large tropical positive biases and extratropical negative biases can compensate, the root mean square error (hereafter RMSE) is a better indicator of the distance to observations, and the mean bias is more useful from a freshwater budget perspective. RMSE also increases from 1.13 mm/day in ERA15 to 1.31 mm/day in ERA40. In subsequent reanalyses, both mean bias and RMSE decrease as a result of the reduction in tropical precipitation. Although ERA-Interim and ERA5 have similar mean biases (0.24 mm/day in ERAinterim, 0.23 mm/day in ERA5), the distance to observations appears to be much reduced in ERA5, which is reflected in the RMSE numbers (0.90 mm/day in ERA-Interim, 0.64 mm/day in ERA5). Li et al. (2021) attributes the reduction of tropical precipitation over the western Pacific in ERA5 to the decrease in convective precipitation. The study focuses on the role of the improved ice water path from the updated convection scheme in IFS. Nogueira (2020) also shows the important role of deep convection in improving ERA5 tropical precipitation and link the rainfall increase at mid-latitude with better moisture flux convergence.

The zonal mean precipitation, shown in Figure 3, highlights the role of the tropics and extratropics. Zonal means are shown for the whole available period for each data set to stay consistent with previous figures. Results are comparable when averaged over the common period (1979–1993) and do not differ by more than a few percent. All ECMWF reanalyses overestimate precipitation in the tropics (defined here from 25° *N* to 25° *S*) but their meridional structures agree well with observational estimates. ERA40 has the most intense precipitation at the height of the ITCZ (in excess of 8 mm/day), which is reduced in newer products to approximately 7 mm/day. GPCP estimates are 6 mm/day, but there is still uncertainty about the exact magnitude. Other products, such as TRMM, offer larger estimates of just under 7 mm/day over their available period (1998–2018). Interestingly, ERA15 is not far from ERA5 in the tropical band (on zonal average) due to the compensation of biases along the equator in South America and the maritime continent, leading to a tropical bias of only 0.66 mm/day. In comparison, ERA40 has a bias of 1.07 mm/day, ERA-Interim 0.73 mm/day, and ERA5 0.44 mm/day. In the extratropics (defined here from 25° to 75° for both hemispheres), all but ERA5 exhibit a deficit in the modeled precipitation, but of lesser amplitude. Here, ERA15 performs quite poorly, particularly in the southern hemisphere. Each successive generation improves over the previous, with error shrinking from −0.33 mm/day in ERA15 to 0.07 mm/day in ERA5 in the southern hemisphere and from −0.24 mm/day to 0.07 mm/day in the northern hemisphere, respectively, for ERA15 and ERA5. The precipitations of ERA5 agree very well with GPCP, except for the overestimation of the local minima at 25° *N* and 25° *S*. A local maximum at 60° *S* is shown in

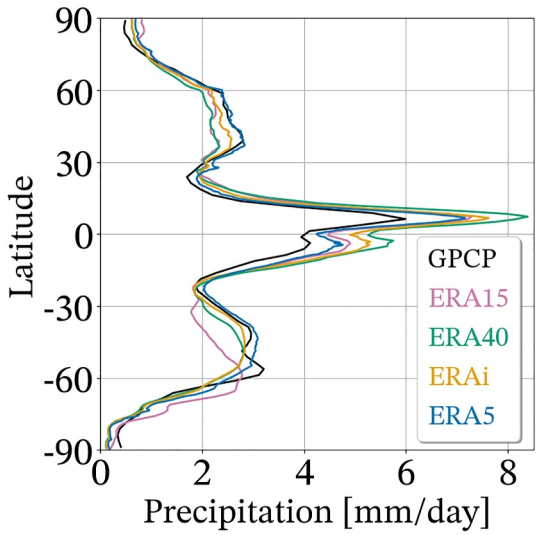

Figure 3. Zonal average of the climatological annual mean precipitation in GPCP (1979–2020), ERA15 (1979–1993), ERA40 (1958–2001), ERA-Interim (1979–2018) and ERA5 (1979–2020). All data sets are presented at their native resolutions.

the GPCP estimates but does not exist in the updated GPCP v3.2 (Huffman et al., 2023) or in CMAP (Xie & Arkin, 1997). Adler et al. (2003) acknowledges the limitations of satellite retrievals at high latitude based only on cloudiness. In the polar regions, the reanalyses are biased with opposite signs: positive in the northern hemisphere, negative in the southern hemisphere. GPCP v2.3 estimates about the same amount of precipitation over both poles, whereas the reanalyses simulate a wetter Arctic and dryer Antarctic.

From the globally averaged precipitation time series shown in Figure 4, it appears in GPCP estimates that the long-term mean is 2.7 mm/day, the standard deviation (measure of interannual variability) of the annual mean global precipitation (weighted by area) is 0.024 mm/day, and its trend is +0.006 mm/day/decade, equivalent to a net increase in precipitation of 0.024 mm/day between 1979 and 2019, comparable to one standard deviation. All reanalyses overestimate long-term mean precipitation by at least 0.2 mm/day (approximately 7%), which is consistent with the uncertainty reported by Adler et al. (2018). Adler et al. (2020) also reported that studies of Behrangi et al. (2014), Rodell et al. (2015), and Trenberth et al. (2014) adjust GPCP precipitation by up to 5% to close the water cycle. Biases between ECMWF reanalyses and GPCP are more than twice as large as differences between precipitation estimates. For reference, the global average of TRMM blended with GPCP at high latitudes is shown to only depart from the GPCP global average by less than 0.1 mm/day. ERA15 and ERA40 exhibit very large interannual fluctuations, with standard deviations of 0.13 and 0.26 mm/day, respectively. Despite an overestimated interannual variability, the trend of ERA15 is 0.008 mm/day/decade and is in good agreement with GPCP. ERA40 begins with values comparable to GPCP in 1958, but quickly exceeds the observed global mean and finishes largely above the observed values with more than 3.4 mm/day. This is equivalent to a trend of 0.176 mm/day/*decade* for the entire period and of 0.255 mm/day/decade over the later 1979–2001 period. ERA-Interim benefits from the lessons learned from ERA40 and provides a more stable time serie. Interannual variability is greatly reduced to 0.061 mm/day (2.5 times greater than GPCP) and is largely driven by three successive trends: first of −0.058 mm/day/decade during 1979–2005, followed by an abrupt 0.423 mm/day/*decade* during 2005–2010 and −0.078 mm/day/decade afterward. The cause of these spurious trends has been identified by Dee et al. (2011) as originating in the assimilation of rain. The resulting trend over the entire period is in agreement with GPCP, but this highlights the limitation of a linear trend fit. Finally, the trend in ERA5 during the same period (1979–2022) is 0.036 mm/day/decade despite having values similar to those of ERA-Interim at both ends of the time series. Although ERA5 does not show trends as pronounced as ERA-Interim, it starts with a −0.048 mm/day/decade decline during 1979–1992 followed by a steady increase of 0.052 mm/day/decade over the remaining years. The reduction in the magnitude of the partial trends leads to a standard deviation of 0.046 mm/day, more in agreement with GPCP but still twice as high. The correlation between the global time series of ERA reanalyses and GPCP ranges from −0.54 in ERA15 to 0.48 in ERA5, but it is not a correct metric to determine the representation of interannual variability due to compensatory or additive biases.

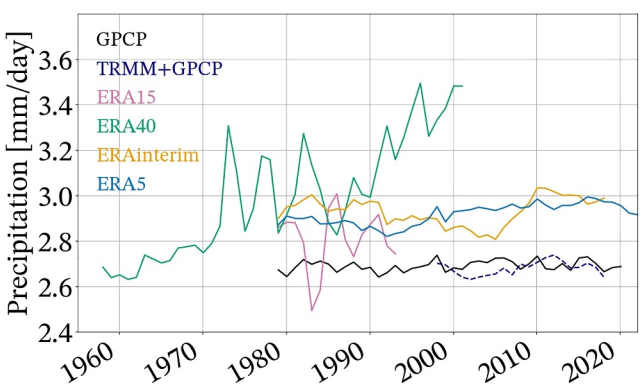

Figure 4. Global mean precipitation (annual average) in GPCP, ERA15, ERA40, ERA-Interim and ERA5. TRMM + GPCP is a blend of TRMM where it exists ($50°N - 50°S$) augemented with GPCP values at high latitudes.

A better assessment of the realism of interannual variability can be obtained with the correlation between the detrended annual time series of the modeled and observed precipitation. Figure 5 shows that the interannual variability in the Equatorial Pacific has been well captured in all reanalyses, and is where the correlation is highest because precipitation anomalies are dominated by ENSO (Dai & Wigley, 2000). Other areas with high correlation are desert and dry regions, which have low interannual variability. Among the regions with the worst representation of interannual variability are CAF, the subtropical South-East Pacific, and the polar regions. These are consistent with the lower correlation between ERA5 and weather stations in the tropics (Lavers

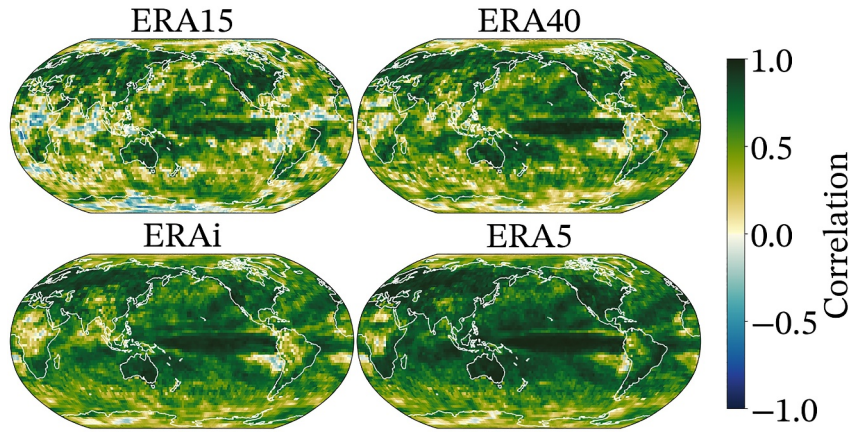

Figure 5. Correlation between ERA15 (1979–1993), ERA40 (1979–2001), ERA-Interim (1979–2018), ERA5 (1979–2020) and GPCP. ERA data sets are coarsened onto GPCP grid with conservative remapping then the Pearson's R is computed on the detrended annual timeseries of modeled versus observed precipitation.

et al., 2022), for which the handling of convective systems and orography are likely culprits. At high latitudes, few rain gauge observations are available to constrain both satellite estimates or atmospheric models, and precipitation is generally small compared to the tropics and extra-tropics. The evolution of the correlation between all generations of ERA re-analyses shows an incremental improvement. The improvement is not homogeneous and there are many spatial structures in the correlation fields, which complicates the interpretation of such maps. The area-weighted mean correlation coefficients provide a global estimate of how well the reanalyses correlate with observations. The values for all reanalyses are: 0.46 for ERA15, 0.51 for ERA40, 0.62 for ERA-Interim and 0.70 for ERA5. The values for ERA-Interim and ERA5 agree with the values reported by Hersbach et al. (2020) in their comparison with TRMM, for which the correlation for ERA5 was 0.7, up from 0.63 in ERA-Interim. Using monthly time series artificially improves the correlation, with values 0.07 (ERA5) to 0.14 (ERA15) higher than the annual correlation, because the seasonal cycle is typically both well captured and the dominant signal of the time series. The use of an area-weighted average is not ideal because subsidence zones, for example, in the eastern Pacific and Atlantic, have poor correlation, little rain, and yet a large surface area. Therefore, their contribution to the final correlation may not be as relevant to judge the accuracy of a modeled data set.

Precipitation trends, a signal that slowly varies beneath interannual variability, are of particular interest for the climate community because of their environmental impacts and the "dry gets drier, wet gets wetter" assertion is the object of many studies, such as Greve et al. (2014) or Feng and Zhang (2015). Adler et al. (2020) shows a northward shift of the ITCZ in the Pacific Ocean and increased precipitations in the SPCZ and Indian Ocean and that these changes appear to follow the pattern of change in column water vapor (see their Figure 35.6). Figure 6 presents the trends obtained in all ERA reanalyses as well as the trends in GPCP for the corresponding period. Hatches are superimposed where the trend is significant. Significance is obtained with a two-tailed Student's *t* test with the null hypothesis that the first and second half of each time series have equal mean with 95% confidence. The trend obtained for GPCP for 1979–2020 is consistent with the results of Adler et al. (2020), but it is worth noting that the trend is significant only in limited geographical areas. The precipitation trend in ERA15 suffers from an alternance of strong negative and positive trends in the tropics and general drying of the mid-latitudes, with significant trends in places where GPCP does not show statistical significance. ERA40 solved the problem of mid-latitudes drying, but the tropical oceans (in particular the western Pacific and Indian) have a strong positive trend, worsened by the wrong interpretation of radiances after the Mount Pinatubo eruption, as explained by Dee et al. (2011). It also shows statistical significance in many oceans where GPCP does not. ERA-Interim and ERA5 have results in better agreement with GPCP although the areas of significance do not coincide. For example, ERA-Interim and ERA5 produce significant trends in South America, CAF, and East Asia. In contrast, GPCP has significant trends in the Southern Ocean (SOO) that ERA-Interim and ERA5 do not capture. Trends and significance for ERA-Interim and ERA5 are consistent with those presented in Figure 12 of Nogueira (2020), but the difference from GPCP presented there appears to use the union of significant trends for both GPCP and ERA-Interim/ERA5 and leads to the conclusion that there is "no clear improvement in rainfall flux trend patterns

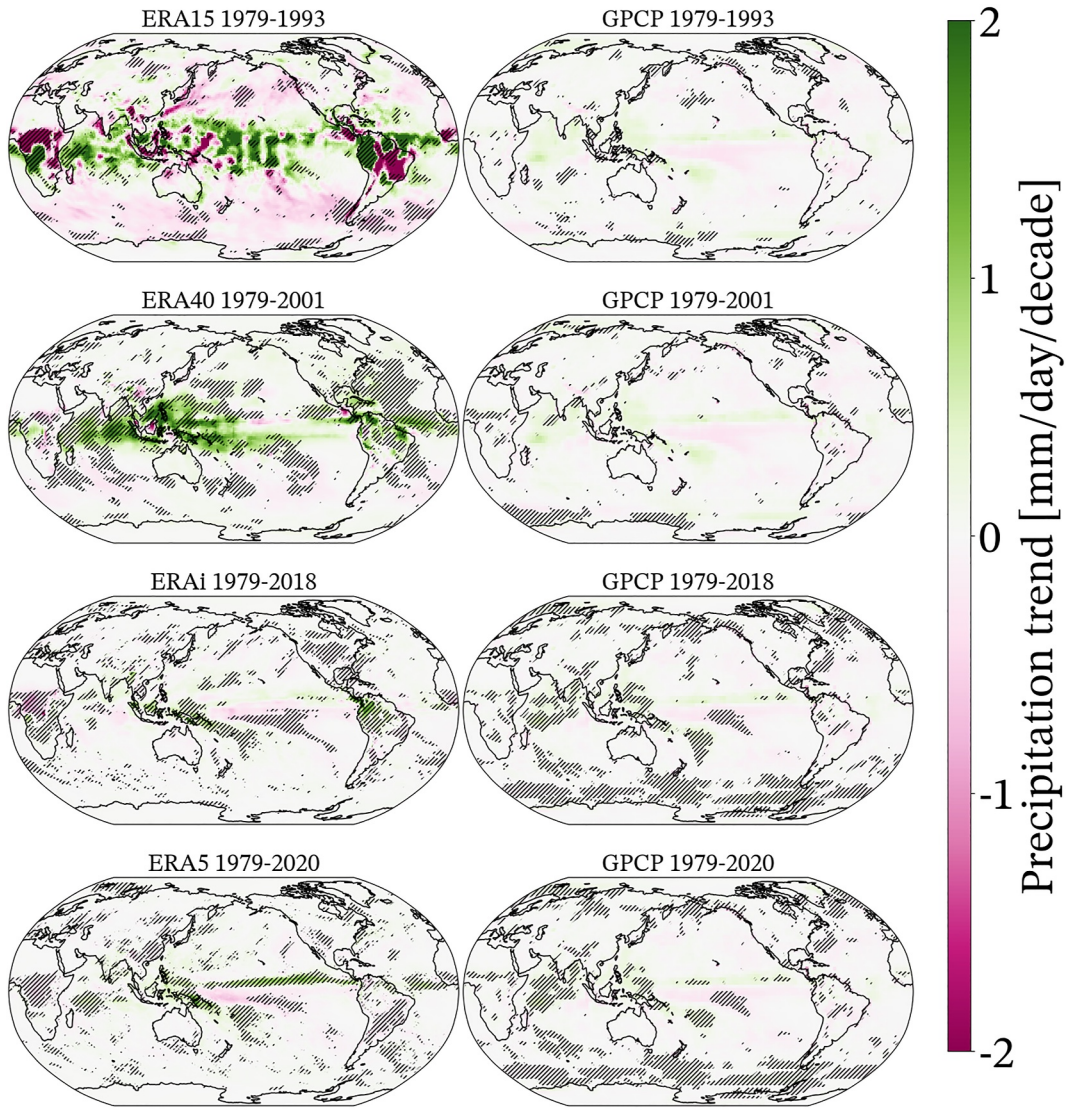

Figure 6. Precipitations trends (mm/day) in reanalyses and in GPCP for corresponding periods. Hatches represent areas of significant trend based on student *t*-test. All data sets are presented at their native resolutions.

between ERA-Interim and ERA-5." Because the trend maps are noisy and the statistical significance is spotty, it is hard to draw hard conclusions regarding improvements between ERA-Interim and ERA5, and various geographical areas see their trend either improve or worsen compared to GPCP.

Global analysis shows progress in representing precipitation between earlier generations of reanalyses (ERA15/ERA40) and the more recent ERA-Interim and ERA5. The comparison between ERA15 and ERA40 shows no significant improvement, but rather the exchange of one set of issues for another. Since ERA40, the representation of mean, interannual variability, and trends has improved greatly. ERA5 outperforms ERA-Interim by all global metrics considered. However, further analysis is limited by the noise and lack of significance in the correlation and trend maps, respectively. Global metrics are heavily influenced by the tropics, as they have the highest amount of precipitation, the largest biases, and their interannual variability is dominated by ENSO, the strongest mode of variability. As reanalyses improve, it may not be as clear how much progress is made in the extratropics if global metrics are mostly reflecting the realism of the tropics. This suggests that there is a need for metrics of intermediate spatial scale in order to present a more detailed, yet comprehensible, picture of the representation of precipitation in the reanalyses.

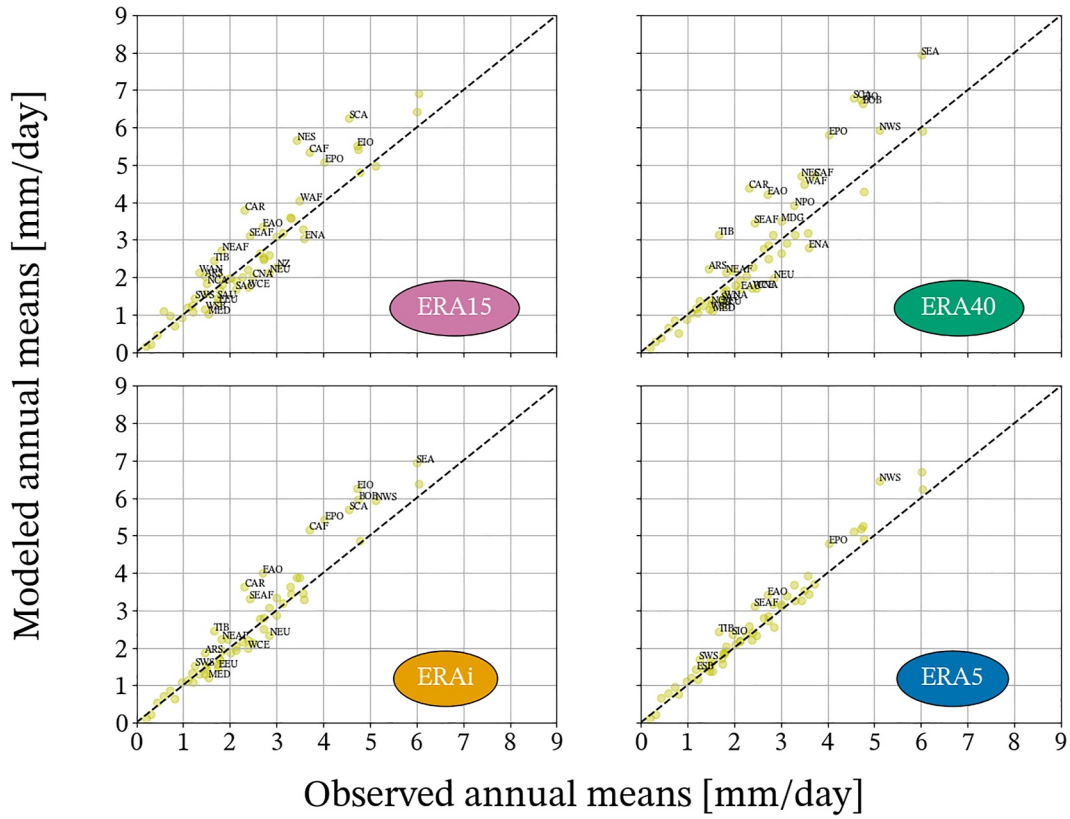

Figure 7. Means in modeled versus observed precipitation for all AR6 regions. Dashed line is unity line. For clarity, abbreviations for regions are only displayed when bias is greater than 15% and mean precipitation is greater than 1 mm/day. The number of regions above the threshold for ERA15, ERA40, ERA-Interim and ERA5 is respectively 25 (CNA, ENA, NCA, SCA, CAR, NES, SWS, NEU, WCE, EEU, MED, WAF, CAF, NEAF, SEAF, WSB, TIB, SAU, NZ, WAN, EPO, EAO, SAO, ARS, EIO), 28 (WNA, CNA, ENA, NCA, SCA, CAR, NWS, NES, NEU, WCE, EEU, MED, WAF, CAF, NEAF, SEAF, MDG, WSB, TIB, SEA, EAU, SAU, NPO, EPO, EAO, ARS, BOB, EIO), 18 (SCA, CAR, NWS, SWS, NEU, WCE, EEU, MED, CAF, NEAF, SEAF, TIB, SEA, EPO, EAO, ARS, BOB, EIO) and 8 (NWS, SWS, SEAF, ESB, TIB, EPO, EAO, SIO).

3.2. Regional Analysis

Separation of data sets into regions is achieved using the list of 58 polygons defined by Iturbide et al. (2020) and used for the IPCC Sixth Assessment Report (AR6). These regions have been selected to separate various geographical areas according to their climatic homogeneity, based on both air temperature and precipitation, and are shown in Figure A1. The target horizontal resolution for the design of these updated regions is 1°, which is comparable to or greater than all ERA reanalyses, but is also suitable for a 2° coarser resolution, such as GPCP, according to Iturbide et al. (2020). To avoid errors due to remapping, the reduction into regions is performed at the native resolution of each data set using the predefined polygons. For compactness, all regions are plotted as scatter plots with observed values on the horizontal axis and modeled values on the vertical axis. Each point on scatter plots represents a region and only outliers are reported by printing their abbreviations on the figures and the full list is available in the captions. The colors indicate the mean precipitation observed in all scatter plots, except in Figure 7. The scatter plots are best interpreted as "score cards," and further analysis is limited by the fact that regions cannot be considered as independent samples from a statistical perspective. This representation allows counting and identifying regions that depart significantly from the unity line and/or exhibit a singular behavior.

3.2.1. Climatological Mean and Seasonal Cycle

Figures 7 and 8 compare the modeled annual mean precipitation and the amplitude of the seasonal cycle (defined as the difference between the maximum and minimum values of the climatological seasonal cycle) with the GPCP observational estimates for all AR6 regions. The average seasonal cycles for all individual regions are available in

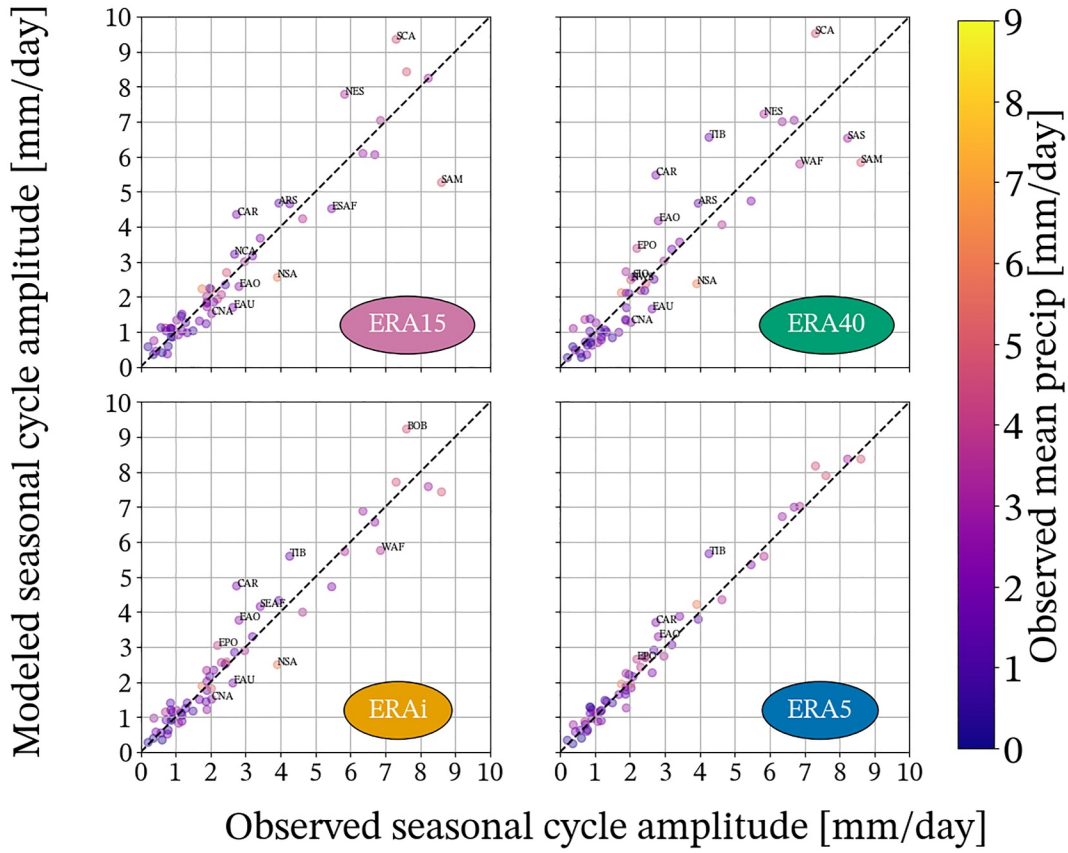

Figure 8. Amplitude in modeled versus observed amplitude of the precipitation seasonal cycle for all AR6 regions. Dashed line is unity line. For clarity, abbreviations for regions are only displayed when the error on seasonal cycle is greater than 15% and the amplitude is the seasonal cycle is greater than 2 mm/day. The number of regions above the threshold for ERA15, ERA40, ERA-Interim and ERA5 is respectively 11 (CNA, NCA, SCA, CAR, NSA, NES, SAM, ESAF, EAU, EAO, ARS), 16 (CNA, SCA, CAR, NWS, NSA, NES, SAM, WAF, TIB, SAS, EAU, EPO, EAO, ARS, BOB, SIO), 10 (CNA, CAR, NSA, WAF, SEAF, TIB, EAU, EPO, EAO, BOB) and 4 (CAR, TIB, EPO, EAO).

the annex Figures A2 and A3. See also Tables A1 and A2 for tabular data on mean annual bias and errors in the representation of the seasonal cycle and abbreviations.

The first takeaway is the general improvement (i.e., a cloud of dots closer to the 1:1 line) from ERA40 to ERA-Interim and then from ERA-Interim to ERA5, both in terms of mean and seasonal cycle. ERA15 and ERA40 have a large number of regions (respectively, 25 and 28 out of 58) where the annual mean precipitation deviates by more than 15% of the observed values (only for regions with an annual mean greater than 1 mm/day). This number is subsequently reduced to 18 in ERA-Interim and finally to 8 in ERA5. The comparison between ERA15 and ERA40 shows a mix of improvement and degradation consistent with the results of Figure 2. The improvement in ERA40 over ERA15 is limited to four regions in the southern hemisphere such as southwest South America (SWS), New Zealand (NZ), West Antarctica (WAN) and southern Atlantic Ocean (SAO) but is accompanied by the degradation of tropical regions, such as Southeast Asia (SEA), the Bay of Bengal (BOB), or eastern Pacific Ocean (EPO). Although ERA-Interim has improved over ERA40 in terms of global bias, 18 regions remain above the arbitrarily chosen 15% threshold. ERA-Interim underestimates mean precipitation over a large area of Europe, northern and eastern (NEU and EEU), western and central, and the Mediterranean Sea (MED) but this is improved in ERA5. Of the 14 regions identified with a large positive bias in ERA-Interim, all but northwest South America (NWS) see a reduction in their bias. This improvement covers a wide range of climates, with annual mean precipitation between 2 and 6 mm/day. Precipitation in NWS increased in ERA5 during April to October compared to ERA-Interim, resulting in a greater positive bias. Some regions remain challenging, such as the equatorial Atlantic and Pacific oceans (EAO and EPO), southeastern Africa (SEAF) and

the Tibetan plateau (TIB). Two regions see a small degradation between ERA-Interim and ERA5: the South Indian Ocean and eastern Siberia (ESB).

With a few exceptions, all reanalyses are able to capture the timing of the average seasonal cycle (see Figures A2 and A3). ERA15 is the only reanalysis with timing issues and only in a few regions. In this case, the maximum of the seasonal cycle in northern North America (NWN and NEN) and the Russian Far East is delayed. It performs rather poorly in many regions of the southern hemisphere, such as southern South America (SSA), the southern Atlantic and Pacific Oceans (SAO and SPO), and down to the SOO and East and West Antarctica (EAN and WAN). In the intriguing case of New Zealand, all reanalyses show a seasonal cycle much larger than the GPCP observations. Across all reanalyses, equatorial regions have a weak and well-captured seasonal cycle, but consistently overestimate precipitation. In regions with larger seasonal cycle, the seasonal minimum is usually in agreement with observations, but the maximum is either under- or overestimated and is the major contributor to the annual bias. Figure 8 shows that most regions have a seasonal cycle amplitude below 3 mm/day and agree well with the observations. The regions for which the error in the seasonal cycle is greater than 15% and the amplitude is greater than 2 mm/day are highlighted. ERA15, ERA40 and ERA-Interim have 10 or more regions above this threshold and distributed on both sides of the unity line, and there are modest improvements between these first two generations and ERA-Interim. ERA5 greatly improves the representation of the seasonal cycle over ERA-Interim, with only four regions crossing the threshold. Of the regions with a weaker than observed seasonal cycle, western Africa (WAF) and northern South America (NSA) show some remarkable improvement. All regions, except the Tibetan Plateau (TIB), see the overestimation of their amplitude reduced: the BOB and southeast Africa (SEAF) are now below the threshold, but the equatorial Atlantic (EAO), Pacific (EPO) and Caribbean (CAR) remain skewed toward higher amplitudes. From a climatological perspective, ERA5 performs the best out of all the considered reanalyses because it captures better the maximum of the seasonal cycle, hence reducing the annual bias for regions with a strong seasonal cycle and is closer to the observed average for regions with a more stationary bias, such as in the equator. This is consistent with the results from the global analysis, which highlighted the role of improved convection and moisture convergence as drivers for more realistic precipitation as shown by Nogueira (2020) and Li et al. (2021).

3.2.2. Trends and Interannual Variability

According to GPCP, almost all AR6 regions in GPCP have trends of magnitude less than 0.10 mm/day/decade. Only the Arabian Sea (ARS), the equatorial Indian Ocean (EIO), and the BOB have higher positive (wetting) statistically significant trends, and only Madagascar (MDG) and the South American monsoon (SAM) have higher negative (drying) significant trends. Of the 58 defined AR6 regions, 28 have a positive trend and 30 have a negative trend (see Table A3 for all tabular data), but only 12 to 13 are statistically significant. The regions with weaker significant positive (wetting) trends are western Siberia (WSB), the Russian Arctic (RAR), and southern South America (SSA). The regions with weaker significant negative (drying) trends are western Antarctica (WAN), northwest North America (NWN), the Tibetan plateau (TIB), western North America (WNA), and the North Atlantic Ocean. The precipitation trends in ERA15 are strongly overestimated in both directions, with 11 regions exceeding 0.10 mm/day/decade and wetting up to 3.88 mm/day/decade in northwest South America (NWS) and 19 regions exceeding −0.10 mm/day/decade and drying to −1.62 mm/day/decade for the SAM. Of the 11 regions with statistically significant trends in ERA15, none agrees in value and significance with the corresponding GPCP trend. Although ERA40 does not model such excessive trends, 48 of the 15 regions have a wetting trend, including 26 in which the trend is greater than 0.10 mm/day/decade and statistically significant for 13 of them. The only two regions for which ERA40 and GPCP agree on the significance and sign of the regional trend are the BOB and the ARS. The other 21 regions where ERA40 has a significant trend do not match either the significance (for 20 of them) or the sign (incorrect wetting trend in Madagascar). Tropical regions have an overestimated wetting trend due to problems in the humidity analysis (spurious increments in the data assimilation system) and interpretation of radiance, as reported in Uppala et al. (2005), but extra tropical regions are also affected. Twenty-six regions with observed negative trends are modeled with a positive trend and as high as 0.65 mm/day/decade for the equatorial Pacific Ocean (EPO).

In ERA-Interim, the magnitudes of excessive trends are reduced even further. Only northern and northwestern South America (NSA and NWS) have wetting upwards of 0.3 mm/day/decade and CAF has a drying trend of −0.44 mm/day/decade. West Africa (WAF) also has an overestimated drying trend of lesser value. Trends are statistically significant in 18 regions (vs. 12–13 in observations), but only roughly agree with GPCP in two of

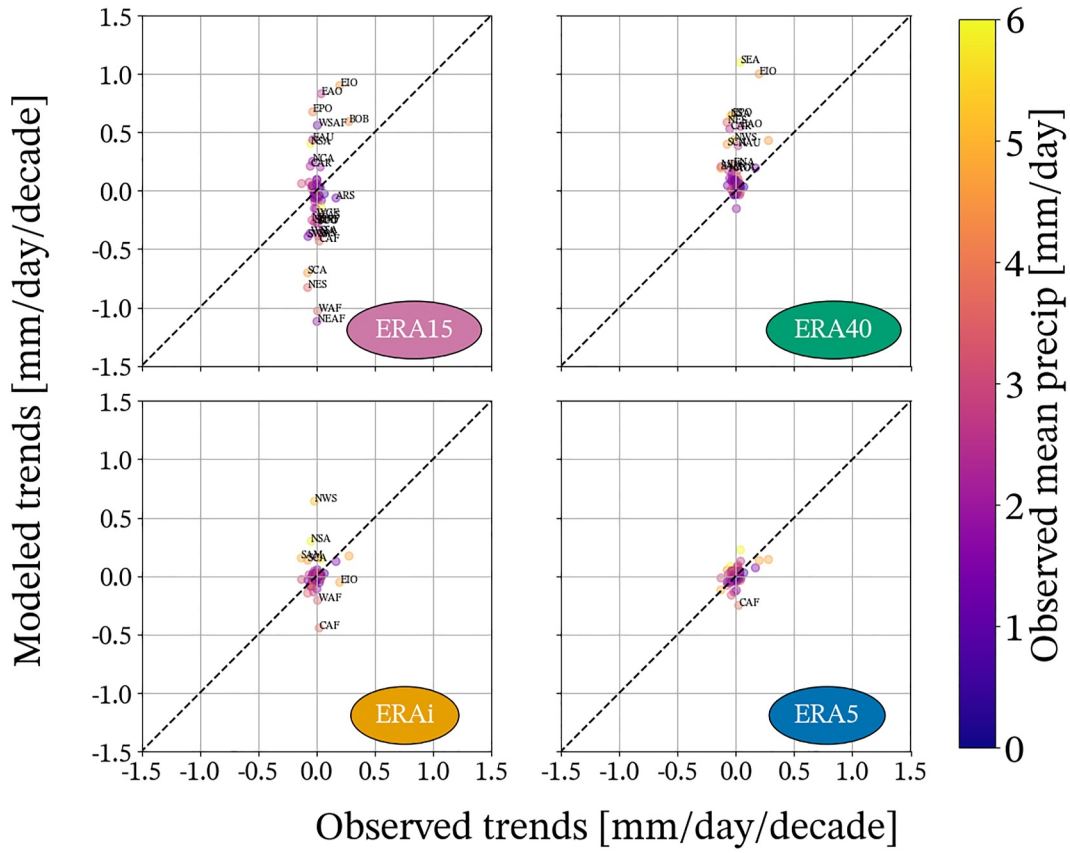

Figure 9. Precipitation trends in ERA15 (top-left), ERA40 (top-right), ERA-Interim (bottom-left) and ERA5 (bottom-right) compared to trends in GPCP. Color is the annual mean precipitation. Dashed line is unity line. For clarity, abbreviations for regions are only displayed when the error on the trend is greater than 0.2 mm/day/decade. The number of regions above the threshold for ERA15, ERA40, ERA-Interim and ERA5 is respectively 27 (WNA, NCA, SCA, CAR, NWS, NSA, NES, SAM, SWS, SSA, WCE, WAF, CAF, NEAF, SEAF, WSAF, RFE, EAS, SAS, EAU, NZ, EPO, EAO, ARS, BOB, EIO, SOO), 15 (CNA, ENA, SCA, CAR, NWS, NSA, NES, SAM, MDG, SEA, NAU, EPO, NAO, EAO, EIO), 7 (SCA, NWS, NSA, SAM, WAF, CAF, EIO) and 1 (CAF).

them: the ARS and WNA. In 24 regions, the trend has opposite signs between ERA-Interim and GPCP, sometimes with large discrepancies, such as in the EIO or the SAM. ERA5 has much weaker regional trends, with only seven regions with absolute values greater than 0.10 mm/day/decade. It overestimates the drying trend in three African regions (CAF, NEAF, and SEAF) and in southeast South America (SES) but also underestimates the wetting trend in the BOB, EIO and ARS. Of 23 statistically significant regional trends, 6 are consistent with GPCP, which is not many but the best so far, and 20 regions have the opposite sign trend. Figure 9 illustrates the progress made in the modeled trends compared to the observation-based ones. ERA15 has 27 regions where the modeled trend has an error greater than 0.2 mm/day/decade (which is comparable to the largest observed regional trend). The large drying trends are then eliminated in ERA40, which is consistent with the overall wet trend in this reanalysis, and the large positive trends remain for 15 regions. ERA-Interim has a more neutral distribution of trends with roughly equal numbers of trends over- and underestimated by 0.2 mm/day/decade or more, for a total of seven, but the spread of error on trends is about the same as ERA40. Finally, in ERA5 only CAF has an error greater than 0.2 mm/day/decade and overestimated drying. This is a large threshold, comparable to some of the largest observed trends, and highlights how far off modeled regional trends have been in early-generation reanalyses and that they have improved between ERA-Interim and ERA5, albeit by a small number of regions.

Although trends are difficult to represent, the interannual variability in the various reanalyses is in much better agreement with the GPCP observations (see Figures A4 and A5 for individual annual time series for each region), except for a few special cases. Even if ERA15 largely overestimates interannual variability in a small number of

regions, such as northeastern Africa (NEAF), the SAM, or the EIO, there are a large number of regions where the solution is in reasonable agreement with observations. Despite its problem with an overall wet trend, ERA40 is also able to capture many features of interannual variability even in regions that are biased, such as southeast Asia (SEA) or the equatorial Pacific Ocean (EPO). ERA-Interim is in good agreement with GPCP in most regions but fails to adequately capture some regions such as northeastern and CAF (NEAF and CAF) or northwest South America (NWS). ERA5 appears to provide time series consistent with observations in most regions. For a more quantitative analysis, it is useful to define a metric for interannual variability as the standard deviation of the detrended annual time series for each region. Figure 10 shows how the modeled interannual variability compares with the observed variability. The observed range of values ranges from 0.03 mm/day in the very consistently dry region of the Sahara to $0.64 - 0.73$ mm/day in the equatorial Pacific Ocean, which is heavily influenced by ENSO (see Table A4 for all tabular data). Regions of lesser variability (under 0.25 mm/day) are, for the most part, well represented or weakly underestimated. Regions with greater interannual variability are more likely to have overestimated variability, particularly in the case of ERA15 and ERA40, which have, respectively, 18 and 17 regions with errors greater than 0.1 mm/day in interannual variability. ERA-Interim clearly improves the modeled interannual variability with only three regions above this threshold: Central and northeastern Africa (CAF and NEAF) have a modeled value twice that observed, and the BOB is 25% higher than the GPCP estimate. ERA5 is closest to observations with only one region above the threshold (southern Central America, SCA). This results in a greater number of regions with high correlation with the observed values (see Table A5 for individual correlations). ERA15 has up to 20 regions with $R < 0.5$ and this number has been reduced with every new iteration to only 5 in ERA5. Newer reanalyses outperform their predecessors in increasing the number of highly correlated regions. There are 24 regions with $R > 0.9$ in ERA5 compared to 12 in ERA-Interim and only 7 in ERA15 and ERA40. ERA40, ERA-Interim, and ERA5 have between 15 and 17 regions with $0.8 < R < 0.9$, while ERA15 only has 11. These numbers indicate that for most regions, ERA5 performs better than the global correlation $R = 0.7$ and the improvement from $R = 0.67$ in ERA-Interim results in a doubling of the number of regions with $R > 0.9$.

3.3. Freshwater Balance of ERA5 in a Global Ocean Model

Because ERA5 has greatly improved precipitation statistics over the previous generation ERA-Interim, evaluating the freshwater balance obtained in a forced ocean model is necessary to decide whether corrections need to be applied for ocean modeling applications. Atmospheric reanalyses often need to be adjusted in order to close the ocean heat and freshwater budgets, as shown in Large and Yeager (2004), Dussin and Barnier (2013) or Tsujino et al. (2018). The evaluation is carried out using a series of experiments using the MOM6 ocean model with global 1/4° horizontal resolution OM4p25 (Adcroft et al., 2019). Because the horizontal resolutions of ERA5 and OM4p25 are similar, the atmospheric variables and fluxes are remapped onto the model grid using the model's built-in bilinear scheme for all but winds, which use a bicubic scheme. The coupling time step between the ocean/ice and atmospheric forcing is set to one hour, which is the temporal resolution of ERA5. Initial conditions for ocean and sea ice are taken from a 1-year spin-up run, initialized with 1979 conditions from the ORAS5 ocean reanalysis (Zuo et al., 2019) and integrated using strong (5 days) restoring over temperature and salinity throughout the water column (*aka* robust diagnostic). Subsequently, the model was integrated for the 1979–2022 available period of ERA5. The first experiment does not use any freshwater adjustment and allows the sea surface height to drift freely. The second experiment uses freshwater adjustment (total water flux is adjusted to near zero using virtual precipitations), and the third uses both freshwater adjustment and sea surface salinity restoring (SSSr), which is commonly used in forced ocean models to prevent large drifts in sea surface salinity and maintain the strength of the Atlantic Meridionnal Overturning Circulation (e.g., Behrens et al., 2013; Biastoch et al., 2008).

Figure 11 shows the globally average net and latent heat fluxes diagnosed in ERA5 and in the aforementioned suite of ERA5-forced ice/ocean experiments at 1/4° horizontal resolution, with or without net freshwater adjustment (fwa) and SSSr. They are compared to previous 1/4° OM4p25 experiments forced by JRA55 do v1.4 with and without fwa and 1/2° OM4p5 experiments forced by ERA-Interim. As expected, the net freshwater adjustment and the SSSr schemes have little effect on the latent and therefore on the net heat flux. The net heat flux of the numerical experiments is evaluated over the 1995–2022 period, after the model spin-up and the large perturbation introduced by the eruption of Mount Pinatubo in 1993. The average net heat flux obtained for the various experiments ranges from 1.03 to 1.55 W/m^2, which is above the estimate 0.39 W/m^2 of Levitus et al. (2012) and of 0.50 W/m^2 in Loeb et al. (2012), as well as the values of the OM4p25 experiments forced with JRA55 v1.4 contributed to Tsujino et al. (2020) and 1/2° OM4p5 of Dussin (2022), which range from 0.5 to

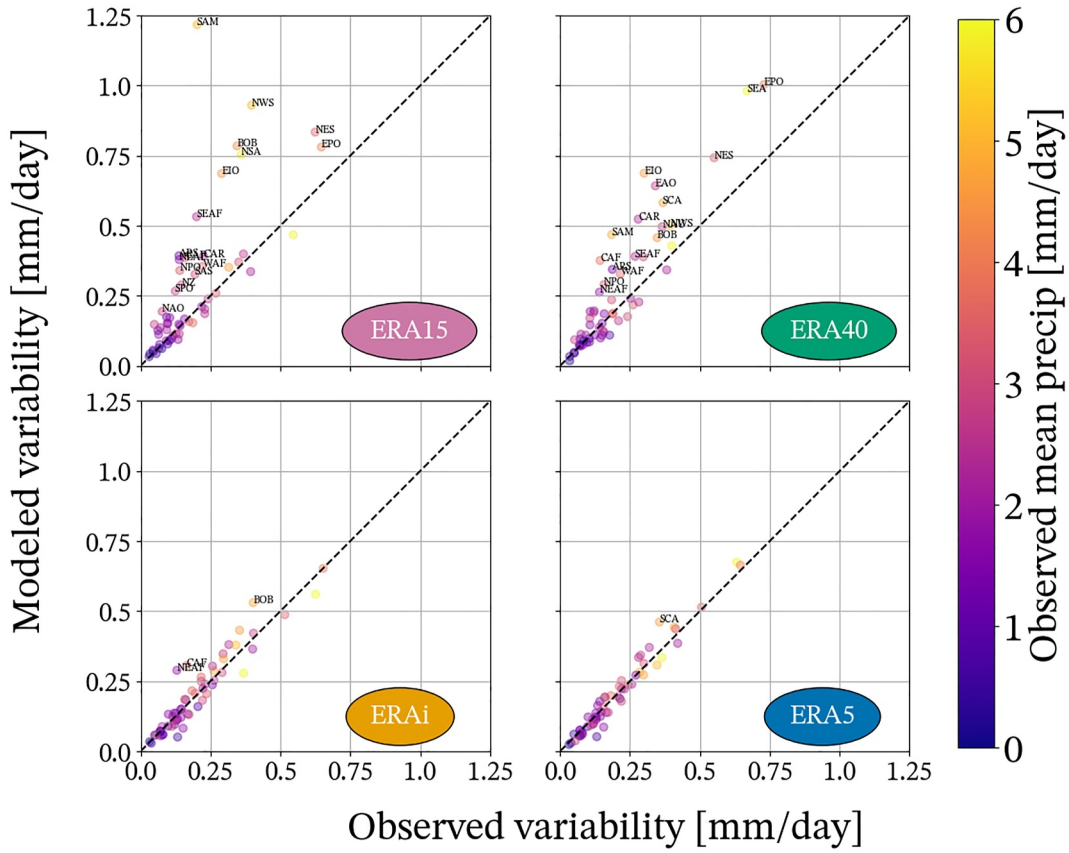

Figure 10. Interannual precipitation variability in ERA15 (top-left), ERA40 (top-right), ERA-Interim (bottom-left) and ERA5 (bottom-right) compared to GPCP. Color is the annual mean precipitation. Dashed line is unity line. For clarity, abbreviations for regions are only displayed when the error on the standard deviation is greater than 0.1 mm/day. The number of regions above the threshold for ERA15, ERA40, ERA-Interim and ERA5 is respectively 18 (CAR, NWS, NSA, NES, SAM, WAF, CAF, NEAF, SEAF, SAS, NZ, NPO, EPO, SPO, NAO, ARS, BOB, EIO), 17 (SCA, CAR, NWS, NES, SAM, WAF, CAF, NEAF, SEAF, SEA, NAU, NPO, EPO, EAO, ARS, BOB, EIO), 3 (CAF, NEAF, BOB) and 1 (SCA).

0.75 W/m^2. The heat and freshwater balances depend on oceanic biases and are specific to each individual model configuration. The overestimated net heat flux leads to some additional ocean warming, but the average sea surface temperature remains stable throughout the simulations and is $0.2 - 0.3°C$ cooler than the OM4 experiments used in Tsujino et al. (2020) and Dussin (2022), which is indicative of a stronger upper ocean mixing. Over the 1995–2017 period, the net solar radiation is 5 W/m^2 stronger in ERA5-forced runs than in JRA55do-forced runs, and consistent with values obtained in the ERA-Interim runs. The net thermal and sensible are respectively 1.1 W/m^2 and 0.5 W/m^2 lower in ERA5-forced runs than in JRA55do-forced runs, which is consistent with a cooler sea surface temperature. This excess heat is partially compensated for by an additional 6.2 W/m^2 of latent heat flux in the ERA5-forced runs. This suggests that some adjustment on the heat fluxes would be necessary to obtain a realistic warming with the OM4p25 configuration forced by ERA5, such as adjusting the downwelling shortwave and longwave radiation to account for the misrepresentation of low-level clouds, as done in Tsujino et al. (2018). In contrast, the net heat flux into the ocean diagnosed directly in ERA5 is much greater: during the 1979–1999 period, the average net heat flux is approximately 11.2 W/m^2 then sharply drops to about 5.6 W/m^2. This is largely due to the 5.4 W/m^2 increase in latent heat flux between the two periods (correlation $R = 0.94$). Other fluxes (sensible, net thermal and net solar) show a steady decrease of no more than 2 W/m^2 between 1979 and 2022.

The net freshwater flux to the ocean is compared with the OM4p5 experiments forced by ERA-interim from Dussin (2022) and an OM4p25 experiment derived from the one used in Tsujino et al. (2020) but without freshwater adjustment in Figure 12. During the 1980–2018 period (limited by the availability of ERA interim,

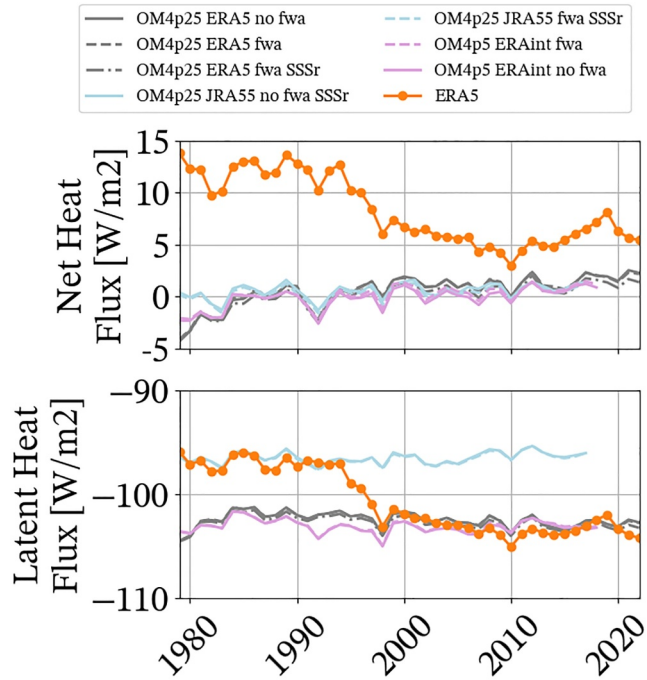

Figure 11. Net and latent heat fluxes in ERA5 (orange) and OM4 experiments forced by ERA5 (gray), JRA55do v1.4 (light blue) and ERA-Interim (light purple). Experiments with (without) net freshwater adjustment are labeled fwa (no fwa) and experiments with sea surface salinity restoring (SSSr) have a SSSr suffix.

1979 is also omitted due to the freshwater imbalance resulting from sea ice spin-up), the experiment forced with JRA55do has a steady net positive freshwater flux of 0.1 mm/day while experiments forced with ERA-Interim and ERA5 have an average deficit of −0.05 mm/day. However, freshwater balances with the ERA-Interim and ERA5 forcing are not as steady over time. OM4p5 forced by ERA-Interim is close to equilibrium during the 1980–1988 period with a net gain of 0.01 mm/day but then has an average deficit of −0.12 mm/day during the 1989–2005 period and then ends with a net gain of 0.05 mm/day during the 2005–2018 period. This behavior is consistent with the global precipitation trends visible in Figure 4. OM4p25 forced by ERA5 has a different evolution: it starts with a net deficit of −0.12 mm/day during the 1980–1999 period, then abruptly increases to be almost in balance (0.01 mm/day) during the 2000–2018 period. This difference can be explained mainly by the 0.14 mm/day increase in precipitation between 1980–1999 and 2000–2018 in ERA5, which does not exist in GPCP observational estimates. In comparison, the net freshwater budget directly diagnosed by ERA5 evaporation, precipitation, and using runoff and calving of the model (about 0.3 mm/day) is closer to balance throughout the period, with a 0.02 mm/day deficit. This balance implies that there is a compensation between both increasing precipitation and evaporation in ERA5.

Figure 13 compares the modeled evaporation with the estimates of OAflux (Yu et al., 2008), SeaFlux v3 (Roberts et al., 2020) and those diagnosed by ERA5 using ECMWF's bulk formula. All data sets have been remapped onto the same 1° horizontal grid and masked where OAflux is not available. There are considerable differences between the observational estimates: the more recent SeaFlux proposes a mean value of 3.67 mm/day during the 1988–2018 period, which is 0.47 mm/day stronger than OAflux. This is largely due to the extension of areas with above average evaporation (between 4 and 6 mm/day) at low and mid latitudes toward the eastern sides of the ocean basins. During the 1988–2000 period, both OAflux and SeaFlux agree on a predominantly positive evaporation trend, except for the $0 - 20\,°N$ band. After 2000, the evaporation trend flattens in SeaFlux while it reverses in OAflux. This is due to the stronger positive specific humidity trend and the negative wind speed trend in OAflux over all low and mid latitudes, resulting in a decrease in evaporation in OAflux. The evaporation diagnosed in ERA5 is in better agreement, both in mean value and trends, with Seaflux estimates.

Evaporation in the OM4 experiments is stronger than OAflux estimates and their 1988–2018 averages range between 3.48 (JRA forcing) and 3.68 mm/day (ERA5 forcing), with little to no differences in the averages over

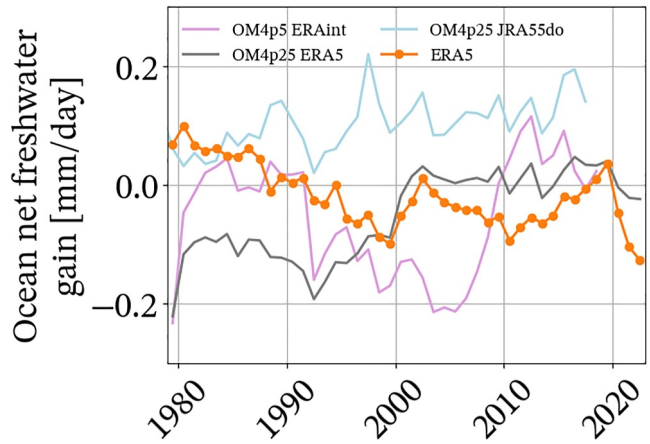

Figure 12. Net freshwater flux into the ocean [mm/day] in experiments forced by JRA55do v1.4, ERA-Interim and ERA5 (gray). No freshwater adjustment has been added to the forcing. In color, net freshwater forcing into the ocean diagnosed from ERA5 precipitation, evaporation and for which the runoff and calving from the model (about 0.3 mm/day) has been added.

1980–1999 and 1999–2018. Although the mean values are better in agreement with the mean evaporation from ERA5 and Seaflux, there is no such agreement on the trend. Since the specific humidity and winds used to calculate the evaporation are the same between ERA5 and OM4 forced by ERA5, this implies that biases in Sea Surface Temperature (used to determine specific humidity at saturation) and different choices for bulk formula can be responsible for the observed discrepancies. Brodeau et al. (2017) showed that changes in algorithms can result in a 10%–15% difference in turbulent heat fluxes, but it is unclear whether this could lead to spurious trends. The comparison of trends between the SST used by ERA5 and OM4 forced by both ERA5 and JRA55 shows that SST trends in the model are weaker in most of the low- and mid-latitudes over the 1988–2000 period, even though they correctly capture the main spatial patterns. The differences between ERA5 SST trends and modeled trends are reduced in subsequent decades, which could explain the better agreement between ERA5 and the modeled evaporation trends after 2000. Modeled SST are most often biased due to various misrepresentations of key ocean dynamics, such as western boundary currents, but no clear pattern or correlation is found between mean SST biases and error in the modeled SST trend. This hints that the problem cannot be reduced to surface processes and that the full three-dimensional circulation needs to be taken into consideration to explain the differences in SST trends, and is beyond the scope of this study. Also, the consistent underestimation of SST trends in both ERA5-

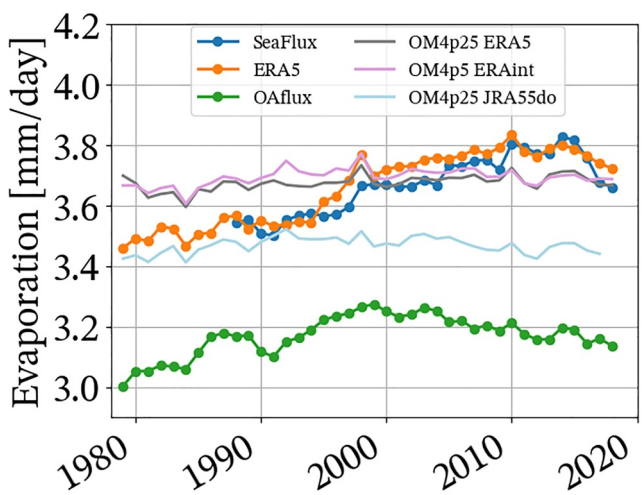

Figure 13. Evaporation [mm/day] in OAflux, ERA5, Seaflux and experiments forced by JRA55do v1.4, ERA-interim and ERA5. All data sets remapped to the 1° grid of Oaflux and masked where OAflux is not defined.

forced and JRA55-forced runs, respectively initialized in 1979 and 1958 suggests the spin-up of the ocean model may not be the cause for such an underestimation.

4. Conclusions

By examining global and regional metrics for modeled precipitations in four generations of ECMWF ERA reanalyses, this study shows that their representation has improved between iterations. The evolution between ERA15 and ERA40 alleviated biases in the southern hemisphere and over steep topographic regions, notably in South America and southeast Asia. Tropical convective precipitation appears to be overestimated in ERA40. ERA40 is the first ECMWF reanalysis to use a 4-D variational assimilation system. Adjustments were made in ERA-Interim to address the assimilation problems identified by (Uppala et al., 2005) using the adaptive bias correction approach of (Dee, 2004). Further improvements since ERA-Interim result in ERA5 being the closest to GPCP observational estimates in all metrics considered.

This evolution is captured by traditional global metrics. Although mean bias and RMSE are worse in ERA40 than in ERA15, spurious trends are mostly reduced and interannual variability moderately improves. ERA-Interim and ERA5 are much closer to observations than ERA40 and ERA15, and ERA5 outperforms ERA-Interim in mean bias, RMSE, and interannual variability. Trends are noisy or are not significant enough to draw robust conclusions. ERA5 overestimates total precipitation by 8.5% versus 5% for ERA15, but the number of regions with absolute errors greater than 15% is reduced by roughly 30%. ERA-Interim and ERA5 have a very similar mean bias, but the RMSE in ERA5 is reduced by 30% and 10 regions see their error drop below 15%. Global precipitation errors are strongly influenced by the tropical precipitation bias and ENSO representation, and the equatorial Pacific is among the regions with the best representation of interannual variability in correlation maps. The global correlation numbers increase from 0.67 to 0.7 between ERA-Interim and ERA5, which can be interpreted as a modest improvement, but also corresponds to a doubling of the regions with a correlation greater than 0.9 and to a majority of regions having correlations greater than 0.8 in ERA5. Regional analysis of trends shows that it is still a challenge to accurately capture observed trends, even in ERA5. However, the number of regions with significant trends in agreement with GPCP increases from 2 to 6 between ERA-Interim and ERA5, contradicting the previous finding of Nogueira (2020) based on trend maps. For example, the regional metrics allowed to identify the EIO and BOB as locations with improved and significant trend between ERA-Interim and ERA5, which is not a straightforward conclusion based on Figure 12 of Nogueira (2020). The regional metrics proposed here offer a useful intermediate spatial scale between often noisy maps and global metrics. They allow one to identify remarkable patterns and allow for a more precise description of a wide range of climates. They also allow one to easily quantify errors in the seasonal cycle and if the bias is stationary or limited to the inadequate representation of the maximum of the seasonal cycle. As the quality of precipitation improves in the next generations of reanalyses, it may be beneficial to include more regional metrics to obtain a more comprehensive picture, which can help interpret the results. Regarding the correction of precipitation to force ocean model, it may be useful to consider using regional metrics as a way to identify any problematic region and correct locally using the most suitable method, or follow the algorithm described in Dussin (2022).

The significant improvement in the representation of precipitation in reanalyses is a great opportunity to assess the quality of the modeled air/sea freshwater fluxes in a modern forced ocean model. The numerical experiments presented here show that it is possible to obtain a more balanced ocean freshwater budget in the last two decades than with JRA55do or ERA-Interim. A more balanced freshwater forcing is beneficial, as it reduces the use of online freshwater adjustment in the model, which produces spurious variability of sea surface salinity (Dussin, 2022). The global trend in ERA5 precipitation can explain the amplitude of the change between the first and last two decades. The ocean model, despite being constrained by ERA5 fluxes, does not reproduce the evaporation trend present in ERA5, which is responsible for maintaining the freshwater balance in ERA5. The assessment of evaporation is complicated by the difference in magnitude and trend in various observational products, but differences in SST trends between modeled and observed SST qualitatively explain the weaker modeled evaporation trends. Inaccuracy in the representation of SST trends can lead to errors in evaporation, and hence freshwater adjustments in ocean models may still be necessary for the time being. Considerable efforts have been made to better understand and represent air/sea fluxes leading to different algorithms such as COARE (Edson et al., 2013; Fairall et al., 1996) or Large and Yeager (2004). Further research is ongoing to both improve the algorithms based on field studies (e.g., Bharti et al., 2019; Bourras et al., 2019; Santini et al., 2020; Song 2021) and their implementation in ocean general circulation models (e.g., Bonino et al., 2022; Brodeau et al., 2017;

Pelletier et al., 2021). If our confidence in the representation of precipitation improves, as this study suggests, then it could become possible in the future to use them to better diagnose the shortcomings of the representation of the rest of the freshwater fluxes in ocean models.

Appendix A: Figures and Tables for Individual Regions

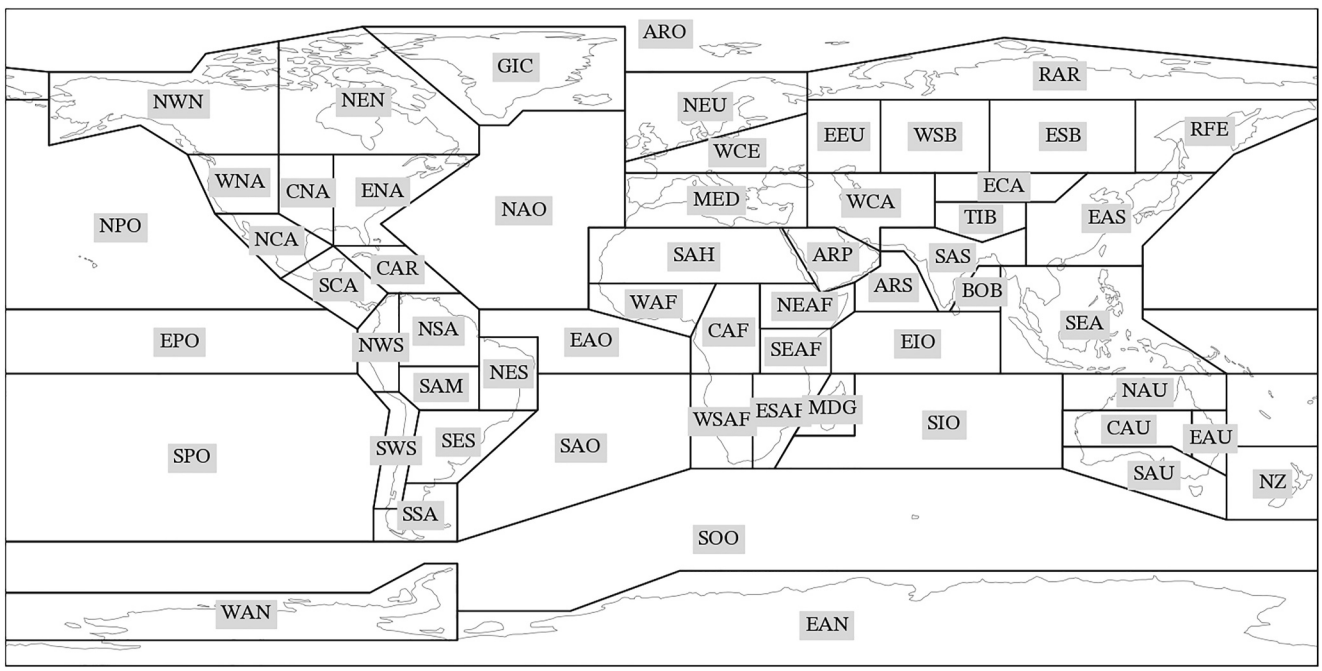

Figure A1. Map of the AR6 scientific regions as defined by Iturbide et al. (2020).

Table A1
Precipitation Bias (mm/day) for Individual Regions

Data set region	ERA15	ERA40	ERAinterim	ERA5	Abbreviations
N.W.South-America	−0.13	0.83	0.82	1.34	NWS
Equatorial.Pacific-Ocean	1.06	1.79	1.41	0.77	EPO
Tibetan-Plateau	0.77	1.46	0.80	0.76	TIB
S.E.Asia	0.41	1.95	0.94	0.71	SEA
Equatorial.Atlantic-Ocean	0.64	1.51	1.29	0.70	EAO
S.Eastern-Africa	0.68	1.02	0.89	0.68	SEAF
S.Central-America	1.68	2.25	1.13	0.56	SCA
Bay-of-Bengal	0.66	1.90	1.21	0.51	BOB
Equatorial.Indic-Ocean	0.79	2.02	1.54	0.47	EIO
S.W.South-America	0.20	0.11	0.26	0.44	SWS
N.Pacific-Ocean	0.30	0.64	0.34	0.39	NPO
S.Indic-Ocean	−0.00	0.22	0.27	0.39	SIO
E.Asia	−0.29	−0.40	−0.11	0.35	EAS
S.Pacific-Ocean	−0.25	0.29	0.22	0.32	SPO
Caribbean	1.48	2.06	1.33	0.26	CAR
S.Asia	0.06	−0.21	0.06	0.25	SAS
E.Siberia	0.06	−0.01	0.15	0.24	ESB
Arctic-Ocean	0.25	0.13	0.15	0.23	ARO
E.C.Asia	0.02	−0.05	0.10	0.23	ECA
E.Antarctica	0.51	0.07	0.13	0.21	EAN
N.South-America	0.87	−0.13	0.34	0.20	NSA
N.W.North-America	−0.02	−0.18	0.07	0.20	NWN
Madagascar	0.10	0.50	0.33	0.16	MDG
N.Atlantic-Ocean	−0.01	0.12	0.13	0.16	NAO
N.E.North-America	0.08	−0.09	0.03	0.15	NEN
N.Australia	−0.20	0.13	0.08	0.13	NAU
W.C.Asia	−0.04	−0.09	0.11	0.13	WCA
New-Zealand	−0.74	−0.36	−0.14	0.12	NZ
South-American-Monsoon	0.01	−0.49	0.07	0.12	SAM
W.Antarctica	0.78	−0.09	−0.04	0.12	WAN
W.Southern-Africa	0.10	−0.05	0.04	0.10	WSAF
N.Eastern-Africa	0.91	0.31	0.42	0.10	NEAF
W.North-America	−0.10	−0.33	−0.07	0.08	WNA
S.South-America	−0.27	−0.23	−0.12	0.08	SSA
Greenland/Iceland	0.21	−0.17	−0.08	0.07	GIC
Russian-Far-East	−0.04	−0.23	−0.16	0.07	RFE
S.Atlantic-Ocean	−0.44	−0.19	−0.09	0.06	SAO
Arabian-Sea	0.57	0.76	0.40	0.05	ARS
N.Central-America	0.32	−0.23	−0.09	0.05	NCA
Western-Africa	0.54	0.98	0.38	0.05	WAF
E.Australia	−0.23	−0.45	−0.18	0.04	EAU
E.Southern-Africa	−0.20	−0.10	−0.18	0.01	ESAF
Southern-Ocean	−0.25	−0.23	−0.22	0.01	SOO

Table A1
Continued

Data set region	ERA15	ERA40	ERAinterim	ERA5	Abbreviations
Central-Africa	1.64	1.00	1.44	−0.00	CAF
S.Australia	−0.29	−0.35	−0.19	−0.02	SAU
S.E.South-America	0.27	−0.17	0.12	−0.03	SES
C.Australia	−0.12	−0.31	−0.18	−0.05	CAU
Russian-Arctic	−0.14	−0.17	−0.14	−0.06	RAR
Sahara	−0.04	−0.10	−0.07	−0.07	SAH
W.Siberia	−0.33	−0.32	−0.17	−0.10	WSB
Arabian-Peninsula	−0.10	−0.02	−0.09	−0.10	ARP
C.North-America	−0.48	−0.78	−0.35	−0.14	CNA
West + Central-Europe	−0.63	−0.68	−0.38	−0.16	WCE
E.North-America	−0.55	−0.80	−0.30	−0.16	ENA
N.E.South-America	2.23	1.26	0.44	−0.16	NES
E.Europe	−0.43	−0.47	−0.28	−0.17	EEU
Mediterranean	−0.51	−0.43	−0.33	−0.17	MED
N.Europe	−0.73	−0.86	−0.52	−0.30	NEU

Note. Each bias is computed with respect to the same time period in GPCP.

Table A2
Ratio of Amplitude of the Modeled Seasonal Cycle (%) to the Observed Seasonal Cycle Over the Same Time Period in GPCP

Region	ERA15	ERA40	ERAinterim	ERA5
New-Zealand	196.8	288.8	256.1	206.1
E.Antarctica	272.0	125.2	130.7	161.1
W.Siberia	129.0	119.0	164.0	151.2
E.C.Asia	97.9	79.4	103.8	145.7
Caribbean	158.5	199.5	172.9	134.9
S.Atlantic-Ocean	102.2	110.0	131.3	133.5
Tibetan-Plateau	109.2	153.7	131.1	132.8
Russian-Arctic	92.9	92.2	124.8	131.6
S.Australia	126.4	158.7	139.1	128.3
E.North-America	156.1	190.1	161.1	122.0
Equatorial.Pacific-Ocean	88.0	153.8	138.4	120.6
N.Pacific-Ocean	106.4	143.7	123.4	118.9
Equatorial.Atlantic-Ocean	81.5	148.1	133.8	117.1
S.W.South-America	98.4	82.1	97.0	115.1
S.Eastern-Africa	107.3	104.1	121.4	113.3
E.Siberia	96.6	89.8	103.6	112.1
S.Central-America	127.9	130.1	105.4	111.7
W.Southern-Africa	113.2	105.6	109.4	111.6
S.E.Asia	126.7	120.6	107.3	110.8
Equatorial.Indic-Ocean	109.6	96.6	104.7	109.7
E.Europe	140.7	97.1	125.8	108.7

Table A2
Continued

Region	ERA15	ERA40	ERAinterim	ERA5
S.Pacific-Ocean	129.3	121.8	115.4	108.6
N.E.North-America	73.0	74.6	105.3	108.5
N.Central-America	119.6	93.0	106.0	108.4
N.South-America	65.3	60.6	63.8	107.7
W.Antarctica	192.7	66.3	93.7	107.4
Madagascar	95.8	110.0	108.2	105.7
Central-Africa	89.2	94.4	110.7	104.9
West + Central-Europe	117.1	66.8	103.6	104.6
N.Australia	90.4	105.1	98.0	104.4
Bay-of-Bengal	110.7	133.1	121.2	103.8
S.Indic-Ocean	88.4	122.3	111.9	103.2
Western-Africa	102.5	84.4	83.9	102.2
S.Asia	100.1	79.3	92.1	101.6
N.W.North-America	86.5	72.1	88.5	100.8
W.C.Asia	125.1	88.0	96.3	100.2
N.Atlantic-Ocean	90.4	110.8	106.3	99.3
E.Southern-Africa	82.6	86.6	86.4	97.9
Russian-Far-East	77.6	58.6	89.1	97.6
South-American-Monsoon	61.2	67.8	86.3	97.2
N.W.South-America	109.2	122.8	89.7	96.4
Arabian-Sea	118.1	118.0	109.4	95.8
N.E.South-America	133.3	123.7	98.1	95.8
N.Eastern-Africa	99.0	104.9	103.0	95.7
C.Australia	68.7	55.4	78.2	94.0
E.Asia	91.2	87.5	86.2	93.9
W.North-America	95.6	88.7	92.5	92.9
S.E.South-America	100.9	101.6	97.4	92.1
C.North-America	74.7	62.5	74.3	90.2
Mediterranean	65.7	72.0	76.8	88.2
E.Australia	64.3	62.7	74.9	85.9
Southern-Ocean	84.4	63.8	76.1	80.8
Arctic-Ocean	74.7	78.1	79.8	80.6
S.South-America	48.0	45.1	67.2	77.3
Greenland/Iceland	127.5	65.2	74.6	76.2
N.Europe	97.3	69.6	64.0	66.5
Arabian-Peninsula	96.0	156.8	107.2	65.7
Sahara	65.6	43.5	56.4	64.7

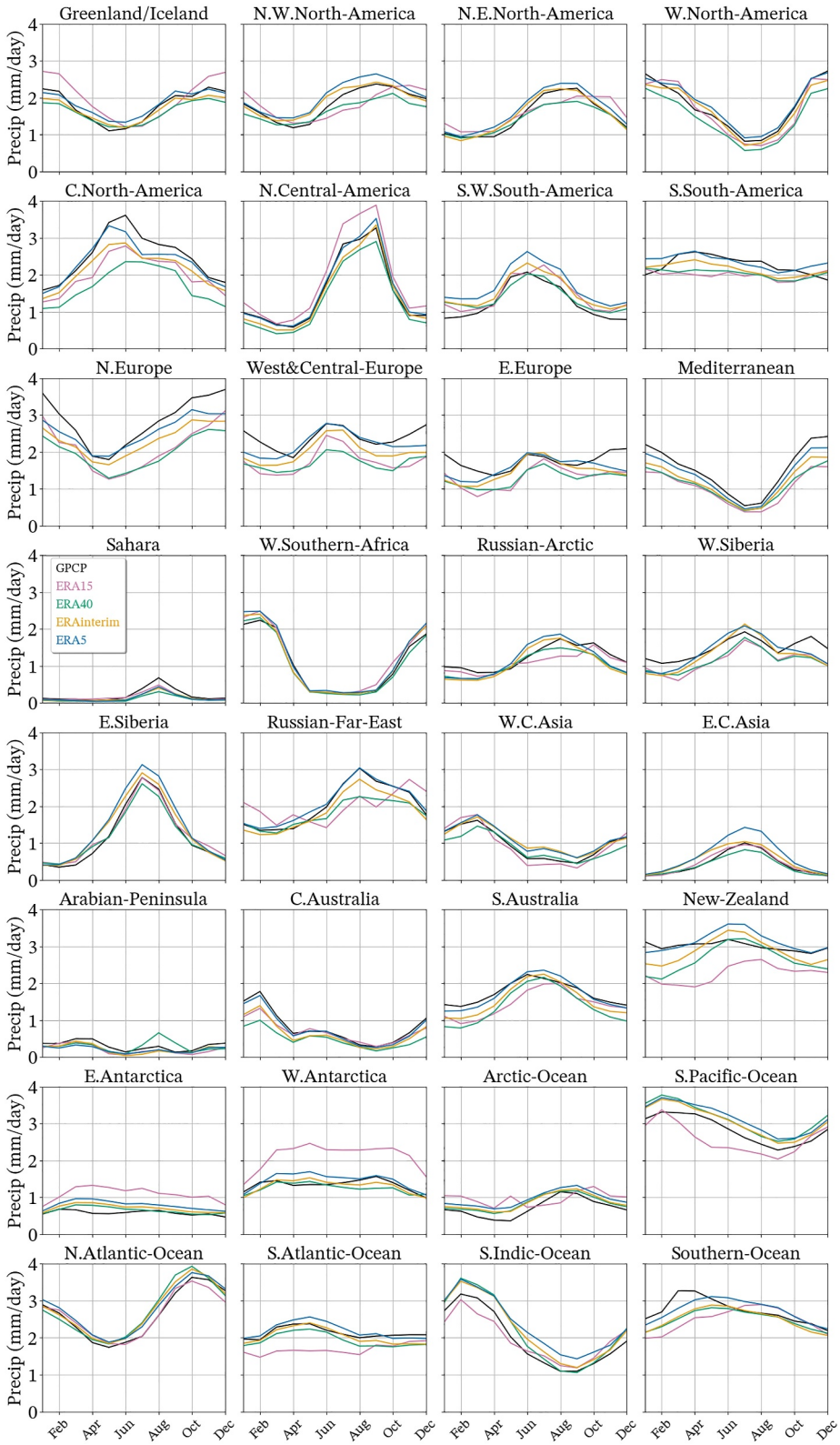

Figure A2. Average seasonal cycle of precipitation (mm/day) for dryer regions.

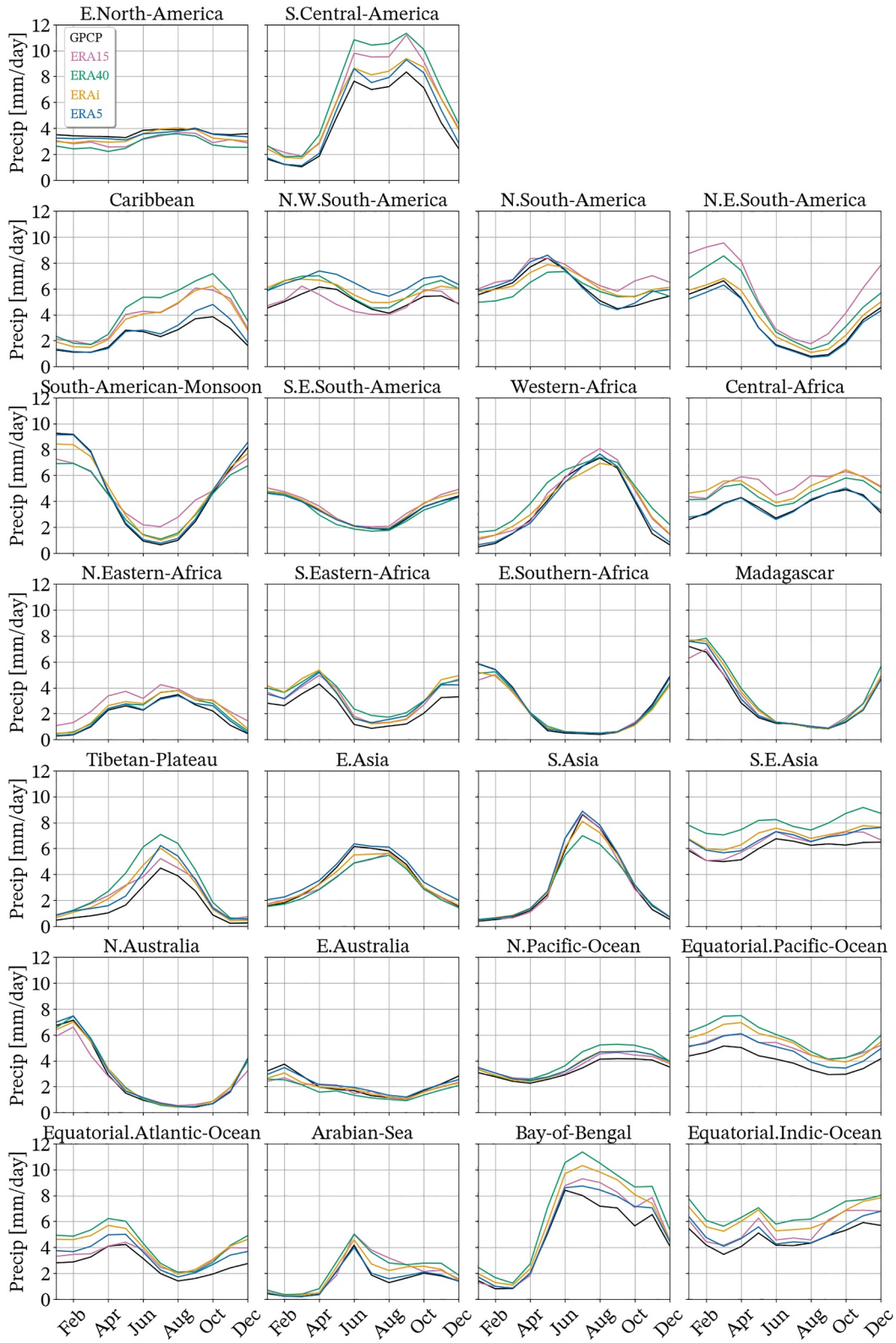

Figure A3. Average seasonal cycle of precipitation (mm/day) for wetter regions.

Table A3
Trends (mm/day/Decade) for AR6 Regions

Region	GPCP 1979–1993	ERA15	GPCP 1979–2001	ERA40	GPCP 1979–2018	ERA interim	GPCP 1979–2020	ERA5
Bay-of-Bengal	0.28	0.59	**0.28**	**0.43**	**0.28**	0.17	**0.28**	**0.14**
Equatorial.Indic-Ocean	0.20	0.90	0.20	**1.00**	**0.20**	−0.05	**0.20**	**0.13**
Arabian-Sea	0.17	−0.06	**0.17**	**0.19**	**0.17**	**0.13**	**0.17**	**0.07**
Arctic-Ocean	0.07	−0.03	0.07	0.03	0.07	0.02	0.07	0.03
W.Siberia	0.04	−0.08	0.04	0.03	**0.04**	−0.00	**0.04**	−0.02
Equatorial.Atlantic-Ocean	0.04	**0.83**	0.04	**0.55**	0.04	0.02	0.04	**0.13**
E.Asia	0.04	−0.23	0.04	−0.02	0.04	−0.02	0.04	**−0.04**
S.E.Asia	0.04	−0.14	0.04	**1.10**	0.04	0.15	0.04	0.22
Russian-Arctic	0.03	0.03	**0.03**	0.03	**0.03**	0.01	**0.03**	**0.03**
S.Indic-Ocean	0.03	**0.20**	0.03	**0.05**	0.03	0.01	0.03	**0.04**
S.South-America	0.03	−0.36	**0.03**	−0.04	**0.03**	−0.03	**0.03**	−0.01
E.Siberia	0.03	−0.05	0.03	**0.06**	0.03	**−0.06**	0.03	**−0.03**
Central-Africa	0.02	−0.43	0.02	**0.09**	0.02	**−0.44**	0.02	**−0.25**
E.C.Asia	0.02	0.03	0.02	0.03	0.02	−0.00	0.02	−0.01
N.Australia	0.02	0.05	0.02	0.38	0.02	0.02	0.02	0.09
S.Pacific-Ocean	0.02	−0.08	0.02	**0.05**	0.02	**0.03**	0.02	**0.04**
Southern-Ocean	0.02	−0.27	**0.02**	−0.02	0.02	0.00	0.02	**0.02**
S.Asia	0.02	−0.39	0.02	0.07	0.02	**0.16**	0.02	0.07
E.Antarctica	0.01	**−0.05**	0.01	0.05	0.01	−0.00	0.01	0.01
Western-Africa	0.01	**−1.03**	**0.01**	0.12	0.01	**−0.21**	0.01	−0.04
N.Pacific-Ocean	0.01	−0.02	0.01	**0.17**	0.01	0.02	0.01	**0.07**
W.Southern-Africa	0.01	**0.56**	0.01	−0.03	0.01	**0.05**	0.01	0.01
Sahara	0.01	−0.06	0.01	−0.01	0.01	−0.02	0.01	−0.00
Russian-Far-East	0.01	**−0.27**	0.01	0.02	0.01	0.01	0.01	0.03
N.Eastern-Africa	0.00	**−1.12**	0.00	**−0.15**	0.00	−0.11	0.00	**−0.12**
Greenland/Iceland	0.00	0.10	0.00	0.06	0.00	0.02	0.00	**0.04**
E.Europe	0.00	0.09	0.00	0.05	0.00	−0.04	0.00	**−0.05**
W.C.Asia	0.00	0.06	0.00	0.04	0.00	**−0.02**	0.00	**−0.03**
Mediterranean	−0.00	−0.15	−0.00	−0.03	−0.00	0.02	−0.00	−0.00
C.Australia	−0.01	−0.04	−0.01	0.09	−0.01	−0.04	−0.01	−0.02
West + Central-Europe	−0.01	−0.22	−0.01	0.02	−0.01	−0.04	−0.01	−0.03
S.Australia	−0.01	−0.02	−0.01	**0.07**	−0.01	−0.01	−0.01	−0.01
W.Antarctica	−0.01	−0.07	−0.01	0.09	**−0.01**	0.00	**−0.01**	0.01
S.Eastern-Africa	−0.01	−0.27	−0.01	0.08	−0.01	0.02	−0.01	**−0.14**
Arabian-Peninsula	−0.02	−0.02	−0.02	−0.04	−0.02	−0.01	−0.02	−0.01
N.Europe	−0.02	−0.09	−0.02	0.07	−0.02	0.02	−0.02	0.03
N.W.South-America	−0.02	**3.89**	−0.02	**0.43**	−0.02	**0.64**	−0.02	**−0.03**
E.Southern-Africa	−0.02	−0.15	−0.02	**−0.03**	−0.02	0.04	−0.02	0.00
E.North-America	−0.02	−0.01	−0.02	**0.22**	−0.02	**−0.04**	−0.02	0.05
S.Atlantic-Ocean	−0.02	−0.03	−0.02	**−0.01**	−0.02	**−0.03**	−0.02	−0.00
C.North-America	−0.02	0.03	−0.02	0.18	−0.02	**−0.14**	−0.02	−0.04
N.E.North-America	**−0.02**	−0.06	**−0.02**	0.07	−0.02	**0.02**	−0.02	**0.03**
E.Australia	−0.03	0.44	−0.03	0.09	−0.03	0.01	−0.03	0.04

Table A3
Continued

Region	GPCP 1979–1993	ERA15	GPCP 1979–2001	ERA40	GPCP 1979–2018	ERA interim	GPCP 1979–2020	ERA5
Equatorial.Pacific-Ocean	−0.03	0.68	−0.03	**0.65**	−0.03	−0.07	−0.03	0.03
N.Central-America	−0.03	0.25	−0.03	**0.15**	−0.03	**−0.04**	−0.03	−0.05
N.W.North-America	−0.03	0.04	−0.03	0.10	**−0.03**	0.01	**−0.03**	0.02
Tibetan-Plateau	−0.04	0.04	−0.04	0.08	**−0.04**	−0.00	**−0.04**	0.04
New-Zealand	−0.04	−0.25	−0.04	**0.01**	−0.04	−0.01	−0.04	0.01
S.E.South-America	−0.04	0.01	−0.04	**0.01**	−0.04	**−0.08**	−0.04	**−0.16**
N.South-America	−0.05	0.40	−0.05	0.64	−0.05	**0.30**	−0.05	0.08
Caribbean	−0.05	0.21	−0.05	0.53	−0.05	−0.09	−0.05	−0.03
W.North-America	−0.05	**−0.36**	−0.05	0.10	**−0.05**	**−0.08**	**−0.05**	**−0.06**
N.Atlantic-Ocean	−0.06	0.07	−0.06	**0.17**	**−0.06**	0.01	**−0.06**	**0.02**
S.W.South-America	−0.07	**−0.39**	−0.07	0.04	−0.07	−0.03	−0.07	−0.05
S.Central-America	−0.07	**−0.70**	−0.07	**0.40**	−0.07	0.14	−0.07	0.05
N.E.South-America	−0.07	−0.83	−0.07	0.58	−0.07	−0.15	−0.07	−0.08
Madagascar	−0.13	0.06	**−0.13**	**0.21**	**−0.13**	−0.03	−0.13	−0.02
South-American-Monsoon	−0.13	−1.62	**−0.13**	0.19	−0.13	**0.15**	**−0.13**	**−0.12**

Note. Bold values mean that the trend is significant based on a student two-tailed *t*-test of a null hypothesis that the first and second half of the time series have equal mean with a 95% confidence.

Table A4
Standard Deviation (mm/day) of Annual Precipitation for AR6 Regions

Region	GPCP 1979–1993	ERA15	GPCP 1979–2001	ERA40	GPCP 1979–2018	ERAinterim	GPCP 1979–2020	ERA5
Equatorial.Pacific-Ocean	0.65	0.78	0.73	1.00	0.65	0.65	0.65	0.66
S.E.Asia	0.55	0.47	0.67	0.98	0.63	0.56	0.63	0.67
N.E.South-America	0.62	0.83	0.55	0.74	0.52	0.49	0.51	0.51
E.Australia	0.39	0.34	0.38	0.34	0.40	0.36	0.42	0.39
N.Australia	0.24	0.24	0.37	0.50	0.40	0.42	0.41	0.44
Bay-of-Bengal	0.35	0.78	0.35	0.46	0.40	0.53	0.41	0.44
N.South-America	0.36	0.75	0.40	0.43	0.37	0.28	0.36	0.33
S.Central-America	0.32	0.35	0.37	0.58	0.35	0.43	0.36	0.46
N.W.South-America	0.40	0.93	0.39	0.50	0.34	0.38	0.35	0.31
Caribbean	0.23	0.39	0.28	0.52	0.32	0.38	0.32	0.37
Madagascar	0.35	0.37	0.30	0.39	0.29	0.28	0.30	0.31
Equatorial.Indic-Ocean	0.29	0.69	0.30	0.69	0.30	0.33	0.30	0.27
Equatorial.Atlantic-Ocean	0.37	0.40	0.34	0.64	0.30	0.35	0.29	0.34
South-American-Monsoon	0.20	1.22	0.18	0.47	0.26	0.29	0.29	0.28
S.Eastern-Africa	0.20	0.53	0.27	0.39	0.26	0.30	0.28	0.34
Arabian-Sea	0.14	0.39	0.19	0.34	0.26	0.24	0.27	0.27
E.Southern-Africa	0.23	0.20	0.28	0.23	0.26	0.25	0.26	0.24
S.E.South-America	0.27	0.26	0.26	0.22	0.24	0.20	0.24	0.24
C.North-America	0.23	0.19	0.21	0.16	0.23	0.24	0.23	0.22
W.North-America	0.22	0.21	0.25	0.24	0.22	0.22	0.22	0.22
S.Asia	0.19	0.33	0.18	0.24	0.22	0.25	0.22	0.25
New-Zealand	0.15	0.29	0.24	0.18	0.22	0.18	0.22	0.18

Table A4
Continued

Region	GPCP 1979–1993	ERA15	GPCP 1979–2001	ERA40	GPCP 1979–2018	ERAinterim	GPCP 1979–2020	ERA5
C.Australia	0.10	0.09	0.18	0.11	0.21	0.16	0.21	0.19
Western-Africa	0.22	0.35	0.22	0.33	0.22	0.26	0.21	0.23
E.Asia	0.17	0.16	0.19	0.19	0.20	0.21	0.21	0.20
E.North-America	0.19	0.15	0.19	0.19	0.18	0.22	0.18	0.20
N.Europe	0.13	0.12	0.15	0.13	0.17	0.13	0.17	0.14
West + Central-Europe	0.14	0.11	0.16	0.12	0.17	0.13	0.17	0.14
Central-Africa	0.16	0.39	0.14	0.38	0.16	0.31	0.16	0.19
N.Central-America	0.16	0.17	0.16	0.19	0.16	0.18	0.16	0.19
Greenland/Iceland	0.13	0.09	0.14	0.10	0.15	0.08	0.16	0.09
N.Pacific-Ocean	0.14	0.34	0.16	0.29	0.16	0.19	0.16	0.16
S.Indic-Ocean	0.10	0.15	0.12	0.20	0.15	0.15	0.15	0.14
E.Europe	0.14	0.15	0.15	0.11	0.14	0.12	0.14	0.12
S.W.South-America	0.14	0.14	0.15	0.15	0.14	0.15	0.14	0.18
N.Eastern-Africa	0.14	0.38	0.14	0.26	0.13	0.29	0.13	0.16
Arctic-Ocean	0.06	0.04	0.07	0.10	0.13	0.05	0.13	0.05
Russian-Far-East	0.12	0.11	0.14	0.14	0.13	0.11	0.13	0.12
Mediterranean	0.09	0.09	0.12	0.11	0.13	0.11	0.13	0.11
S.Australia	0.10	0.15	0.11	0.15	0.12	0.14	0.13	0.14
W.Southern-Africa	0.09	0.17	0.10	0.08	0.13	0.14	0.13	0.12
W.Siberia	0.11	0.10	0.11	0.09	0.12	0.10	0.12	0.10
N.Atlantic-Ocean	0.08	0.19	0.11	0.17	0.12	0.11	0.12	0.10
S.South-America	0.09	0.13	0.09	0.11	0.12	0.12	0.12	0.11
S.Pacific-Ocean	0.12	0.27	0.12	0.19	0.11	0.09	0.11	0.09
Tibetan-Plateau	0.10	0.17	0.11	0.19	0.10	0.13	0.10	0.12
W.C.Asia	0.10	0.08	0.10	0.10	0.10	0.09	0.10	0.09
Russian-Arctic	0.07	0.06	0.07	0.07	0.08	0.06	0.08	0.06
W.Antarctica	0.06	0.13	0.07	0.07	0.08	0.06	0.08	0.07
S.Atlantic-Ocean	0.07	0.14	0.07	0.11	0.08	0.09	0.08	0.06
E.Siberia	0.07	0.08	0.07	0.08	0.07	0.07	0.07	0.08
N.E.North-America	0.04	0.06	0.05	0.05	0.07	0.06	0.07	0.05
N.W.North-America	0.06	0.11	0.08	0.07	0.07	0.07	0.07	0.08
Arabian-Peninsula	0.08	0.06	0.08	0.09	0.07	0.07	0.07	0.06
Southern-Ocean	0.05	0.15	0.05	0.09	0.05	0.06	0.05	0.04
E.C.Asia	0.05	0.05	0.05	0.05	0.05	0.06	0.05	0.06
E.Antarctica	0.03	0.03	0.03	0.03	0.04	0.03	0.04	0.03
Sahara	0.03	0.04	0.03	0.02	0.03	0.03	0.03	0.02

Table A5
Correlation (Pearon's R) of Modeled Interannual Timeseries With GPCP Estimates for AR6 Regions

Region	ERA15	ERA40	ERAinterim	ERA5
E.Australia	0.91	0.90	0.95	0.98
C.Australia	0.78	0.92	0.93	0.98
Equatorial.Pacific-Ocean	0.80	0.89	0.91	0.97
S.E.Asia	0.67	0.83	0.86	0.97
N.Australia	0.80	0.89	0.90	0.97
W.C.Asia	0.81	0.85	0.90	0.97
N.E.South-America	0.91	0.81	0.88	0.97
West + Central-Europe	0.92	0.92	0.94	0.96
E.Southern-Africa	0.82	0.90	0.88	0.96
Mediterranean	0.83	0.92	0.90	0.96
Russian-Far-East	0.86	0.91	0.93	0.96
W.North-America	0.92	0.98	0.93	0.96
W.Siberia	0.89	0.81	0.87	0.95
E.Europe	0.93	0.92	0.90	0.94
Caribbean	0.40	0.90	0.78	0.94
S.W.South-America	0.78	0.85	0.93	0.94
E.Siberia	0.82	0.61	0.87	0.93
S.Eastern-Africa	0.49	0.89	0.81	0.93
N.Central-America	0.74	0.70	0.82	0.92
N.South-America	0.50	0.55	0.78	0.92
E.Asia	0.55	0.67	0.88	0.92
S.Australia	0.55	0.74	0.86	0.91
S.E.South-America	0.81	0.88	0.92	0.90
C.North-America	0.88	0.80	0.76	0.90
Arabian-Peninsula	0.70	0.85	0.81	0.90
S.Asia	0.78	0.73	0.73	0.90
S.Central-America	0.40	0.68	0.56	0.90
E.North-America	0.77	0.83	0.82	0.90
Madagascar	0.38	0.67	0.75	0.89
E.C.Asia	0.81	0.49	0.77	0.87
S.Indic-Ocean	−0.25	0.70	0.76	0.87
N.Europe	0.94	0.87	0.87	0.87
W.Southern-Africa	0.36	0.74	0.66	0.87
Arabian-Sea	0.05	0.41	0.67	0.87
N.W.North-America	0.74	0.83	0.90	0.85
New-Zealand	0.29	0.68	0.69	0.85
N.Atlantic-Ocean	−0.18	0.21	0.64	0.84
South-American-Monsoon	0.22	0.22	0.72	0.84
N.Pacific-Ocean	0.85	0.59	0.72	0.83
Russian-Arctic	0.91	0.87	0.74	0.80
Sahara	0.55	0.73	0.62	0.80
N.E.North-America	0.64	0.18	0.82	0.80
Equatorial.Atlantic-Ocean	0.24	0.61	0.83	0.79

Table A5
Continued

Region	ERA15	ERA40	ERAinterim	ERA5
Tibetan-Plateau	0.71	0.39	0.71	0.79
S.Pacific-Ocean	0.42	0.53	0.72	0.78
Greenland/Iceland	0.70	0.79	0.76	0.77
Bay-of-Bengal	−0.36	0.63	0.45	0.74
N.Eastern-Africa	−0.41	0.39	0.30	0.74
Equatorial.Indic-Ocean	−0.38	0.40	0.31	0.72
S.South-America	0.60	0.70	0.51	0.72
N.W.South-America	0.12	0.28	0.44	0.70
S.Atlantic-Ocean	−0.13	0.55	0.39	0.60
Western-Africa	0.76	0.69	0.61	0.57
Central-Africa	0.56	0.12	0.23	0.45
Arctic-Ocean	0.26	0.33	0.43	0.41
W.Antarctica	0.41	0.24	0.44	0.38
E.Antarctica	0.24	0.47	0.38	0.36
Southern-Ocean	0.27	−0.12	−0.13	0.14

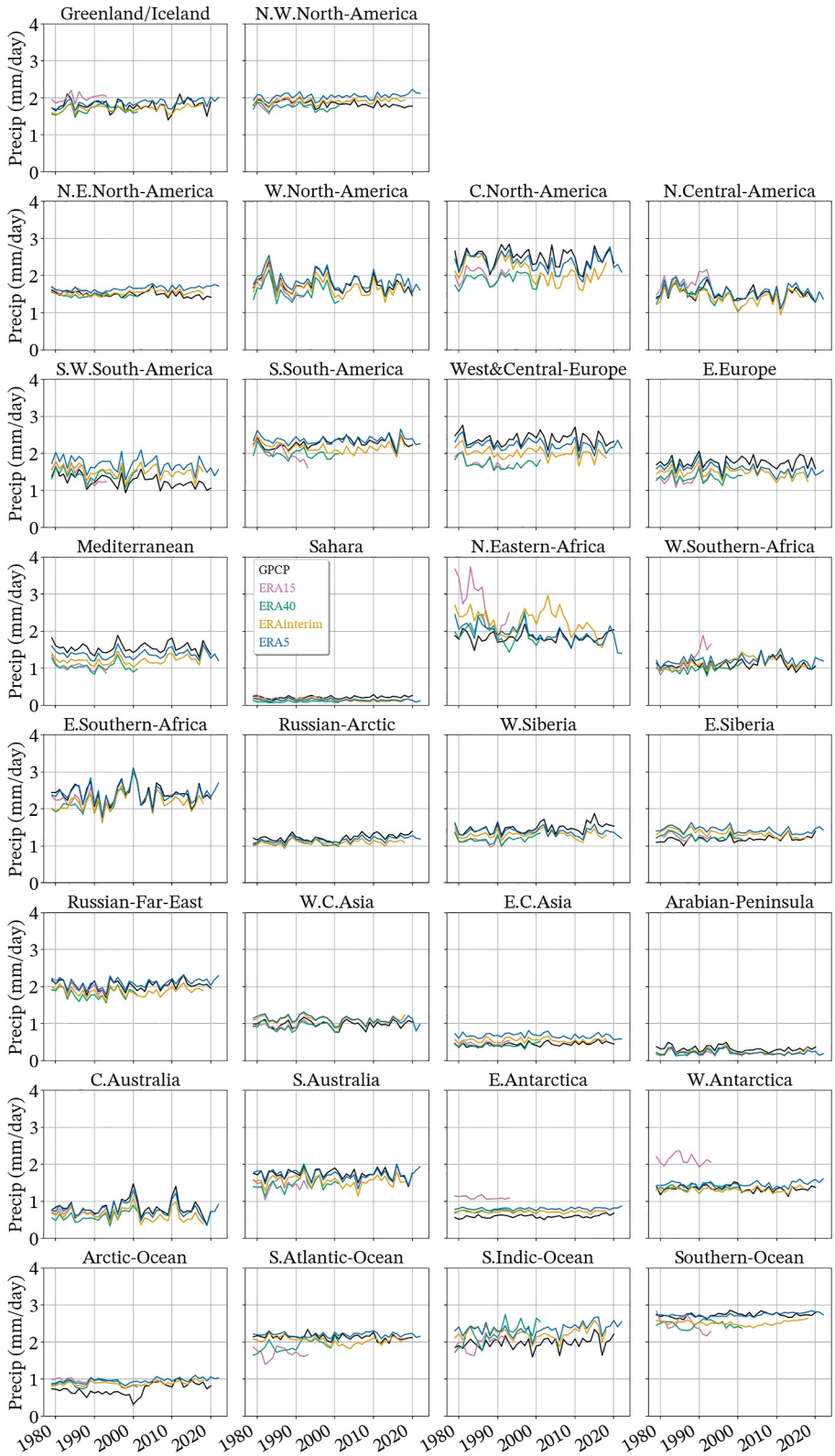

Figure A4. Regional mean precipitation (area-weighted) (mm/day) for dryer regions.

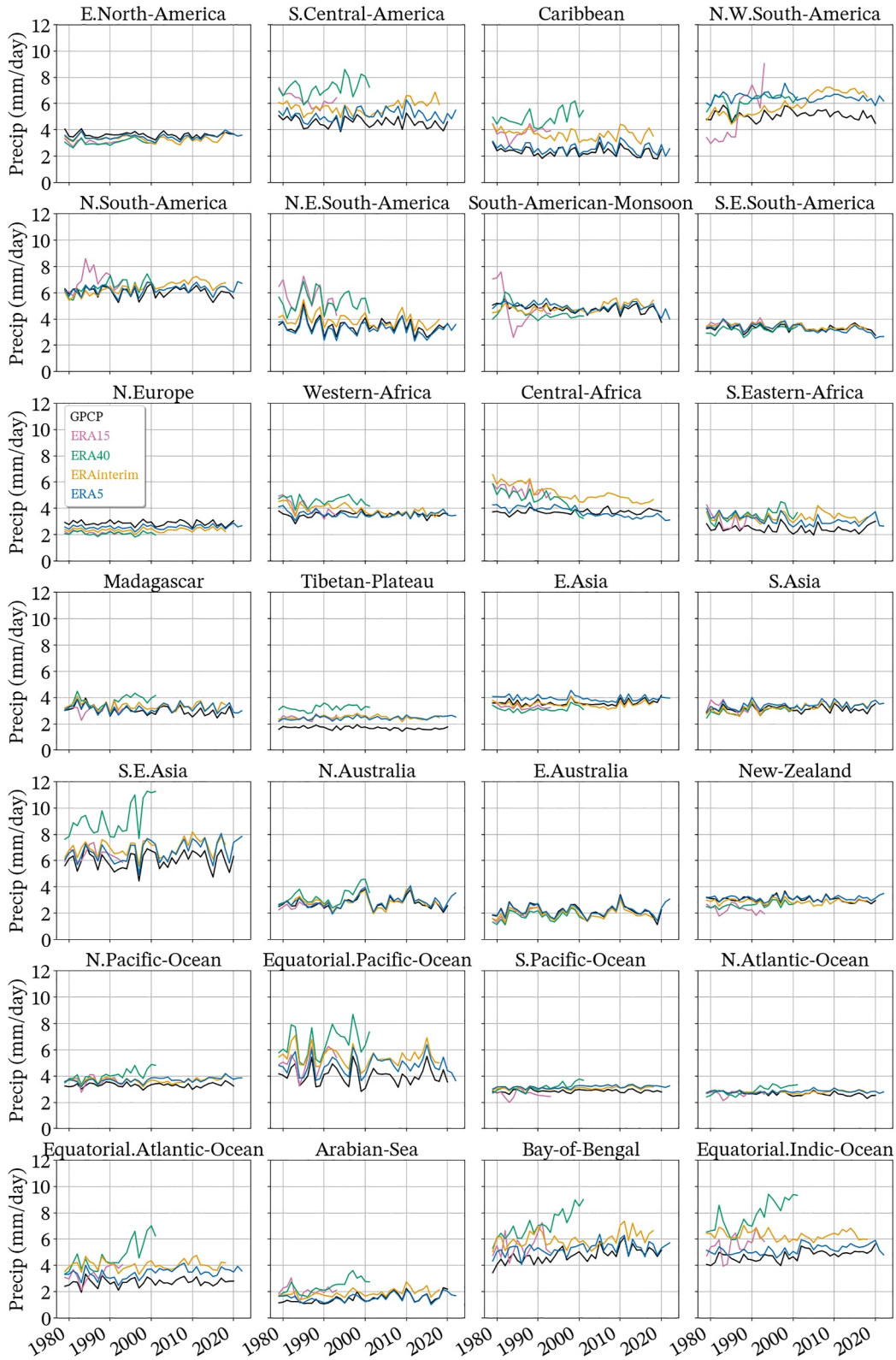

Figure A5. Regional mean precipitation (area-weighted) (mm/day) for wetter regions.

Conflict of Interest

The authors declare no conflicts of interest relevant to this study.

Data Availability Statement

ERA15 (Gibson et al., 1997), ERA40 (Uppala et al., 2005) and ERA-interim (Dee et al., 2011) data are available through the DKRZ (Deutsches Klimarechenzentrum) World Data Center for Climate https://www.wdc-climate.de/ui/ and ERA5 (Hersbach et al., 2020) is available directly from ECMWF at the time of publication https://www.ecmwf.int/en/forecasts/dataset/ecmwf-reanalysis-v5. GPCP v2.3 (Adler et al., 2018) is available from the NOAA National Centers for Environmental Information https://www.ncei.noaa.gov/access/metadata/landing-page/bin/iso?id=gov.noaa.ncdc:C00979. SeaFlux (Roberts et al., 2020) is available from the NASA EarthData portal https://cmr.earthdata.nasa.gov/search/concepts/C1995869798-GHRC_DAAC.html. OAflux (Yu et al., 2008) is available from the Woods Hole Oceanographic Institution (WHOI) pages https://oaflux.whoi.edu/data-access/. The analysis has been carried out using Python and heavily relied on the following packages: numpy (Harris et al., 2020), scipy (Virtanen et al., 2020), xarray (Hoyer & Hamman, 2017), regionmask (Hauser et al., 2024), matplotlib (Hunter, 2007), cartopy (Met Office, 2010–2015) and xESMF (Zhuang et al., 2023). All data and code necessary to reproduce the figures are available on zenodo at https://zenodo.org/records/14032029 (Dussin, 2024).

Acknowledgments
This research from the Geophysical Fluid Dynamics Laboratory is supported by NOAA's Science Collaboration Program and are administered by UCAR CPAESS under award NA21OAR4310383 and NA23OAR4310383B. Many thanks to Liz Drenkard, Matthew Harrison and Enrique Curchitser for their insightful comments, which helped significantly improve the manuscript. Many thanks as well to the two anonymous reviewers for their time providing constructive remarks on this manuscript, which helped clarify certain points of methodology and add important pieces of information.

References

Adcroft, A., Anderson, W., Balaji, V., Blanton, C., Bushuk, M., Dufour, C. O., et al. (2019). The GFDL global ocean and sea ice model OM4.0: Model description and simulation features. *Journal of Advances in Modeling Earth Systems*, *11*(10), 3167–3211. https://doi.org/10.1029/2019MS001726

Adler, R. F., Gu, G., Huffman, G. J., Sapiano, M. R., & Wang, J.-J. (2020). GPCP and the global characteristics of precipitation. *Satellite Precipitation Measurement*, *2*, 677–697. https://doi.org/10.1007/978-3-030-35798-6_11

Adler, R. F., Huffman, G. J., Chang, A., Ferraro, R., Xie, P.-P., Janowiak, J., et al. (2003). The version-2 global precipitation climatology project (GPCP) monthly precipitation analysis (1979–present). *Journal of Hydrometeorology*, *4*(6), 1147–1167. https://doi.org/10.1175/1525-7541(2003)004⟨1147:TVGPCP⟩2.0.CO;2

Adler, R. F., Sapiano, M. R. P., Huffman, G. J., Wang, J.-J., Gu, G., Bolvin, D., et al. (2018). The global precipitation climatology project (GPCP) monthly analysis (new version 2.3) and a review of 2017 global precipitation. *Atmosphere*, *9*(4), 138. https://doi.org/10.3390/atmos9040138

Arkin, P. A., & Xie, P. (1994). The global precipitation climatology project: First algorithm intercomparison project. *Bulletin of the American Meteorological Society*, *75*(3), 401–420. https://doi.org/10.1175/1520-0477(1994)075⟨0401:TGPCPF⟩2.0.CO;2

Behrangi, A., Stephens, G., Adler, R. F., Huffman, G. J., Lambrigtsen, B., & Lebsock, M. (2014). An update on the oceanic precipitation rate and its zonal distribution in light of advanced observations from space. *Journal of Climate*, *27*(11), 3957–3965. https://doi.org/10.1175/JCLI-D-13-00679.1

Behrens, E., Biastoch, A., & Böning, C. W. (2013). Spurious AMOC trends in global ocean sea-ice models related to subarctic freshwater forcing. *Ocean Modelling*, *69*, 39–49. https://doi.org/10.1016/j.ocemod.2013.05.004

Bengtsson, L., & Kållberg, P. (1981). Numerical simulation—Assessment of FGGE data with regard to their assimilation in a global data set. *Advances in Space Research*, *1*(4), 165–187. https://doi.org/10.1016/0273-1177(81)90060-0

Bharti, V., Fairall, C. W., Blomquist, B. W., Huang, Y., Protat, A., Sullivan, P. P., et al. (2019). Air-sea heat and momentum fluxes in the southern ocean. *Journal of Geophysical Research: Atmospheres*, *124*(23), 12426–12443. https://doi.org/10.1029/2018JD029761

Biastoch, A., Böning, C. W., Getzlaff, J., Molines, J.-M., & Madec, G. (2008). Causes of interannual–decadal variability in the meridional overturning circulation of the midlatitude North Atlantic Ocean. *Journal of Climate*, *21*(24), 6599–6615. https://doi.org/10.1175/2008JCLI2404.1

Bonino, G., Iovino, D., Brodeau, L., & Masina, S. (2022). The bulk parameterizations of turbulent air–sea fluxes in NEMO4: The origin of sea surface temperature differences in a global model study. *Geoscientific Model Development*, *15*(17), 6873–6889. https://doi.org/10.5194/gmd-15-6873-2022

Bosilovich, M. G., Chen, J., Robertson, F. R., & Adler, R. F. (2008). Evaluation of global precipitation in reanalyses. *Journal of Applied Meteorology and Climatology*, *47*(9), 2279–2299. https://doi.org/10.1175/2008JAMC1921.1

Bourras, D., Cambra, R., Marié, L., Bouin, M.-N., Baggio, L., Branger, H., et al. (2019). Air-sea turbulent fluxes from a wave-following platform during six experiments at sea. *Journal of Geophysical Research: Oceans*, *124*(6), 4290–4321. https://doi.org/10.1029/2018JC014803

Brodeau, L., Barnier, B., Gulev, S. K., & Woods, C. (2017). Climatologically significant effects of some approximations in the bulk parameterizations of turbulent air–sea fluxes. *Journal of Physical Oceanography*, *47*(1), 5–28. https://doi.org/10.1175/JPO-D-16-0169.1

Brodeau, L., Barnier, B., Treguier, A.-M., Penduff, T., & Gulev, S. (2010). An ERA40-based atmospheric forcing for global ocean circulation models. *Ocean Modelling*, *31*(3–4), 88–104. https://doi.org/10.1016/j.ocemod.2009.10.005

Bukovsky, M. S., & Karoly, D. J. (2007). A brief evaluation of precipitation from the North American regional reanalysis. *Journal of Hydrometeorology*, *8*(4), 837–846. https://doi.org/10.1175/JHM595.1

Dai, A., & Wigley, T. (2000). Global patterns of ENSO-induced precipitation. *Geophysical Research Letters*, *27*(9), 1283–1286. https://doi.org/10.1029/1999GL011140

Dee, D. P. (2004). Variational bias correction of radiance data in the ECMWF system. In *Proceedings of the ECMWF workshop on assimilation of high spectral resolution sounders in NWP, Reading, UK* (Vol. 28, pp. 97–112).

Dee, D. P., Uppala, S. M., Simmons, A. J., Berrisford, P., Poli, P., Kobayashi, S., et al. (2011). The ERA-interim reanalysis: Configuration and performance of the data assimilation system. *Quarterly Journal of the Royal Meteorological Society*, *137*(656), 553–597. https://doi.org/10.1002/qj.828

Dussin, R. (2022). Bias and trend correction of precipitation datasets to force ocean models. *Journal of Atmospheric and Oceanic Technology*, *39*(11), 1717–1728. https://doi.org/10.1175/JTECH-D-22-0007.1

Dussin, R. (2024). Notebooks for Dussin, four generations of ECMWF precipitation…. *Earth and Space Science*. https://doi.org/10.5281/zenodo.12573394

Dussin, R., & Barnier, B. (2013). *The making of Drakkar forcing set 5.1* (Technical Report). MEOM/LEGI.

Edson, J. B., Jampana, V., Weller, R. A., Bigorre, S. P., Plueddemann, A. J., Fairall, C. W., et al. (2013). On the exchange of momentum over the open ocean. *Journal of Physical Oceanography*, *43*(8), 1589–1610. https://doi.org/10.1175/JPO-D-12-0173.1

Fairall, C., Bradley, E., Rogers, D., Edson, J., & Young, G. (1996). The TOGA COARE bulk flux algorithm. *Journal of Geophysical Research*, *101*(C2), 3747–3764. https://doi.org/10.1029/95jc03205

Feng, H., & Zhang, M. (2015). Global land moisture trends: Drier in dry and wetter in wet over land. *Scientific Reports*, *5*(1), 18018. https://doi.org/10.1038/srep18018

Gelaro, R., McCarty, W., Suárez, M. J., Todling, R., Molod, A., Takacs, L., et al. (2017). The modern-era retrospective analysis for research and applications, version 2 (MERRA-2). *Journal of Climate*, *30*(14), 5419–5454. https://doi.org/10.1175/JCLI-D-16-0758.1

Ghajarnia, N., Akbari, M., Saemian, P., Ehsani, M. R., Hosseini-Moghari, S.-M., Azizian, A., et al. (2022). Evaluating the evolution of ECMWF precipitation products using observational data for Iran: From ERA40 to ERA5. *Earth and Space Science*, *9*(10), 1–24. https://doi.org/10.1029/2022EA002352

Gibson, J., Kållberg, P., Uppala, S., Hernandez, A., Nomura, A., & Serrano, E. (1997). *ERA Description (Computer software manual No. 1)*. ECMWF.

Greve, P., Orlowsky, B., Mueller, B., Sheffield, J., Reichstein, M., & Seneviratne, S. I. (2014). Global assessment of trends in wetting and drying over land. *Nature Geoscience*, *7*(10), 716–721. https://doi.org/10.1038/ngeo2247

Harris, C. R., Millman, K. J., van der Walt, S. J., Gommers, R., Virtanen, P., Cournapeau, D., et al. (2020). Array programming with NumPy. *Nature*, *585*(7825), 357–362. https://doi.org/10.1038/s41586-020-2649-2

Hassler, B., & Lauer, A. (2021). Comparison of reanalysis and observational precipitation datasets including ERA5 and WFDE5. *Atmosphere*, *12*(11), 1462. https://doi.org/10.3390/atmos12111462

Hauser, M., Spring, A., Busecke, J., van Driel, M., & Lorenz, R., & readthedocs assistant. (2024). regionmask: version 0.12.1. https://doi.org/10.5281/zenodo.10849860

Hersbach, H., Bell, B., Berrisford, P., Hirahara, S., Horányi, A., Muñoz-Sabater, J., et al. (2020). The ERA5 global reanalysis. *Quarterly Journal of the Royal Meteorological Society*, *146*(730), 1999–2049. https://doi.org/10.1002/qj.3803

Hill, C., DeLuca, C., Balaji, V., Suarez, M., & Da Silva, A. (2004). The architecture of the earth system modeling framework. *Computing in Science & Engineering*, *6*(1), 18–28. https://doi.org/10.1109/MCISE.2004.1255817

Hoyer, S., & Hamman, J. (2017). xarray: N-D labeled arrays and datasets in Python. *Journal of Open Research Software*, *5*(1), 10. https://doi.org/10.5334/jors.148

Huffman, G. J., Adler, R. F., Behrangi, A., Bolvin, D. T., Nelkin, E. J., Gu, G., & Ehsani, M. R. (2023). The new version 3.2 global precipitation climatology project (GPCP) monthly and daily precipitation products. *Journal of Climate*, *36*(21), 7635–7655. https://doi.org/10.1175/JCLI-D-23-0123.1

Huffman, G. J., Bolvin, D. T., Nelkin, E. J., Wolff, D. B., Adler, R. F., Gu, G., et al. (2007). The TRMM multisatellite precipitation analysis (TMPA): Quasi-global, multiyear, combined-sensor precipitation estimates at fine scales. *Journal of Hydrometeorology*, *8*(1), 38–55. https://doi.org/10.1175/JHM560.1

Hunter, J. D. (2007). Matplotlib: A 2D graphics environment. *Computing in Science & Engineering*, *9*(3), 90–95. https://doi.org/10.1109/MCSE.2007.55

Iturbide, M., Gutiérrez, J. M., Alves, L. M., Bedia, J., Cerezo-Mota, R., Cimadevilla, E., et al. (2020). An update of IPCC climate reference regions for subcontinental analysis of climate model data: Definition and aggregated datasets. *Earth System Science Data*, *12*(4), 2959–2970. https://doi.org/10.5194/essd-12-2959-2020

Janowiak, J. E., Gruber, A., Kondragunta, C. R., Livezey, R. E., & Huffman, G. J. (1998). A comparison of the NCEP–NCAR reanalysis precipitation and the GPCP rain gauge–satellite combined dataset with observational error considerations. *Journal of Climate*, *11*(11), 2960–2979. https://doi.org/10.1175/1520-0442(1998)011⟨2960:ACOTNN⟩2.0.CO;2

Kalnay, E., Kanamitsu, M., Kistler, R., Collins, W., Deaven, D., Gandin, L., et al. (1996). The NCEP/NCAR 40-year reanalysis project. *Bulletin of the American Meteorological Society*, *77*(3), 437–472. https://doi.org/10.1175/1520-0477(1996)077⟨0437:TNYRP⟩2.0.CO;2

Kobayashi, S., Ota, Y., Harada, Y., Ebita, A., Moriya, M., Onoda, H., et al. (2015). The JRA-55 reanalysis: General specifications and basic characteristics. *Journal of the Meteorological Society of Japan. Series II*, *93*(1), 5–48. https://doi.org/10.2151/jmsj.2015-001

Large, W. G., & Yeager, S. G. (2004). Diurnal to decadal global forcing for ocean and sea-ice models: The data sets and flux climatologies. Technical Report TN-460+STR (p. 105). https://doi.org/10.5065/D6KK98Q6

Lavers, D. A., Simmons, A., Vamborg, F., & Rodwell, M. J. (2022). An evaluation of ERA5 precipitation for climate monitoring. *Quarterly Journal of the Royal Meteorological Society*, *148*(748), 3152–3165. https://doi.org/10.1002/qj.4351

Lee, D. E., & Biasutti, M. (2014). Climatology and variability of precipitation in the twentieth-century reanalysis. *Journal of Climate*, *27*(15), 5964–5981. https://doi.org/10.1175/JCLI-D-13-00630.1

Levitus, S., Antonov, J. I., Boyer, T. P., Baranova, O. K., Garcia, H. E., Locarnini, R. A., et al. (2012). World Ocean heat content and thermosteric sea level change (0–2000 m), 1955–2010. *Geophysical Research Letters*, *39*(10). https://doi.org/10.1029/2012GL051106

Li, J.-L. F., Xu, K.-M., Richardson, M., Jiang, J. H., Stephens, G., Lee, W.-L., et al. (2021). Improved ice content, radiation, precipitation and low-level circulation over the tropical Pacific from ECMWF ERA-interim to ERA5. *Environmental Research Communications*, *3*(8), 081006. https://doi.org/10.1088/2515-7620/ac1bfe

Loeb, N. G., Lyman, J. M., Johnson, G. C., Allan, R. P., Doelling, D. R., Wong, T., et al. (2012). Observed changes in top-of-the-atmosphere radiation and upper-ocean heating consistent within uncertainty. *Nature Geoscience*, *5*(2), 110–113. https://doi.org/10.1038/ngeo1375

Met Office. (2010–2015). Cartopy: A cartographic python library with a matplotlib interface [Computer software manual]. *Exeter, Devon*. https://scitools.org.uk/cartopy

Ning, S., Wang, J., Jin, J., & Ishidaira, H. (2016). Assessment of the latest GPM-era high-resolution satellite precipitation products by comparison with observation gauge data over the Chinese Mainland. *Water*, *8*(11), 481. https://doi.org/10.3390/w8110481

Nogueira, M. (2020). Inter-comparison of ERA-5, ERA-interim and GPCP rainfall over the last 40 years: Process-based analysis of systematic and random differences. *Journal of Hydrology*, *583*, 124632. https://doi.org/10.1016/j.jhydrol.2020.124632

Onogi, K., Tsutsui, J., Koide, H., Sakamoto, M., Kobayashi, S., Hatsushika, H., et al. (2007). The JRA-25 reanalysis. *Journal of the Meteorological Society of Japan. Ser. II*, *85*(3), 369–432. https://doi.org/10.2151/jmsj.85.369

Pelletier, C., Lemarié, F., Blayo, E., Bouin, M.-N., & Redelsperger, J.-L. (2021). Two-sided turbulent surface-layer parameterizations for computing air-sea fluxes. *Quarterly Journal of the Royal Meteorological Society*, *147*(736), 1726–1751. https://doi.org/10.1002/qj.3991

Prakash, S., Gairola, R., & Mitra, A. (2015). Comparison of large-scale global land precipitation from multisatellite and reanalysis products with gauge-based GPCC data sets. *Theoretical and Applied Climatology*, *121*(1–2), 303–317. https://doi.org/10.1007/s00704-014-1245-5

Rienecker, M. M., Suarez, M. J., Gelaro, R., Todling, R., Bacmeister, J., Liu, E., et al. (2011). MERRA: NASA's modern-era retrospective analysis for research and applications. *Journal of Climate*, *24*(14), 3624–3648. https://doi.org/10.1175/JCLI-D-11-00015.1

Rivoire, P., Martius, O., & Naveau, P. (2021). A comparison of moderate and extreme ERA-5 daily precipitation with two observational data sets. *Earth and Space Science*, *8*(4). https://doi.org/10.1029/2020EA001633

Roberts, C. A. C., Jason, B., & Robertson, F. R. (2020). SeaFlux data products [evaporation] (Tech. Rep.). Dataset available online from the NASA Global Hydrology Resource Center DAAC, Huntsville, Alabama, U.S.A. https://doi.org/10.5067/SEAFLUX/DATA101

Rodell, M., Beaudoing, H. K., L'ecuyer, T., Olson, W. S., Famiglietti, J. S., Houser, P. R., et al. (2015). The observed state of the water cycle in the early twenty-first century. *Journal of Climate*, *28*(21), 8289–8318. https://doi.org/10.1175/JCLI-D-14-00555.1

Santini, M., Souza, R., Pezzi, L., & Swart, S. (2020). Observations of air-sea heat fluxes in the southwestern Atlantic under high-frequency ocean and atmospheric perturbations. *Quarterly Journal of the Royal Meteorological Society*, *146*(733), 4226–4251. https://doi.org/10.1002/qj.3905

Song, X. (2021). The importance of including sea surface current when estimating air-sea turbulent heat fluxes and wind stress in the Gulf Stream region. *Journal of Atmospheric and Oceanic Technology*, *38*(1), 119–138. https://doi.org/10.1175/JTECH-D-20-0094.1

Sun, Q., Miao, C., Duan, Q., Ashouri, H., Sorooshian, S., & Hsu, K.-L. (2018). A review of global precipitation data sets: Data sources, estimation, and intercomparisons. *Reviews of Geophysics*, *56*(1), 79–107. https://doi.org/10.1002/2017RG000574

Tang, G., Clark, M. P., Papalexiou, S. M., Ma, Z., & Hong, Y. (2020). Have satellite precipitation products improved over last two decades? A comprehensive comparison of GPM IMERG with nine satellite and reanalysis datasets. *Remote Sensing of Environment*, *240*, 111697. https://doi.org/10.1016/j.rse.2020.111697

Tian, B., & Dong, X. (2020). The double-ITCZ bias in CMIP3, CMIP5, and CMIP6 models based on annual mean precipitation. *Geophysical Research Letters*, *47*(8). https://doi.org/10.1029/2020GL087232

Trenberth, K. E., Fasullo, J. T., & Balmaseda, M. A. (2014). Earth's energy imbalance. *Journal of Climate*, *27*(9), 3129–3144. https://doi.org/10.1175/JCLI-D-13-00294.1

Tsujino, H., Urakawa, L. S., Griffies, S. M., Danabasoglu, G., Adcroft, A. J., Amaral, A. E., et al. (2020). Evaluation of global ocean–sea-ice model simulations based on the experimental protocols of the Ocean Model Intercomparison Project phase 2 (OMIP-2). *Geoscientific Model Development*, *13*(8), 3643–3708. https://doi.org/10.5194/gmd-13-3643-2020

Tsujino, H., Urakawa, S., Nakano, H., Small, R. J., Kim, W. M., Yeager, S. G., et al. (2018). JRA-55 based surface dataset for driving ocean–sea-ice models (JRA55-do). *Ocean Modelling*, *130*, 79–139. https://doi.org/10.1016/j.ocemod.2018.07.002

Uppala, S. M., Kållberg, P. W., Simmons, A. J., Andrae, U., Bechtold, V. D. C., Fiorino, M., et al. (2005). The ERA-40 re-analysis. *Quarterly Journal of the Royal Meteorological Society*, *131*(612), 2961–3012. https://doi.org/10.1256/qj.04.176

Virtanen, P., Gommers, R., Oliphant, T. E., Haberland, M., Reddy, T., Cournapeau, D., et al., SciPy 1.0 Contributors. (2020). SciPy 1.0: Fundamental algorithms for scientific computing in Python. *Nature Methods*, *17*(3), 261–272. https://doi.org/10.1038/s41592-019-0686-2

Xie, P., & Arkin, P. A. (1997). Global precipitation: A 17-year monthly analysis based on gauge observations, satellite estimates, and numerical model outputs. *Bulletin of the American Meteorological Society*, *78*(11), 2539–2558. https://doi.org/10.1175/1520-0477(1997)078⟨2539:GPAYMA⟩2.0.CO;2

Yu, L., Jin, X., & Weller, R. (2008). Multidecade global flux datasets from the Objectively Analyzed Air-Sea Fluxes (OAFlux) project: Latent and sensible heat fluxes, ocean evaporation, and related surface meteorological variables. Tech. Rep. OAFlux Project Tech. Rep. OA-2008-01.

Zhuang, J., Dussin, R., Huard, D., Bourgault, P., Banihirwe, A., Raynaud, S., et al. (2023). pangeo-data/xesmf: V0.8.2. https://doi.org/10.5281/zenodo.8356796

Zuo, H., Balmaseda, M. A., Tietsche, S., Mogensen, K., & Mayer, M. (2019). The ECMWF operational ensemble reanalysis–analysis system for ocean and sea ice: A description of the system and assessment. *Ocean Science*, *15*(3), 779–808. https://doi.org/10.5194/os-15-779-2019